Radiation induced corrosion of copper

Åsa Björkbacka

KTH Royal Institute of Technology
School of Chemical Science and Engineering
Department of Chemistry
Applied Physical Chemistry
SE-100 44 Stockholm, Sweden

TRITA-CHE Report 2015:57
ISSN 1654-1081
ISBN 978-91-7595-710-4

Akademisk avhandling som med tillstånd av KTH i Stockholm framlägges till offentlig granskning för avläggande av teknologie doktorsexamen onsdagen den 18 november 2015 klockan 10.00 i Kollegiesalen, KTH, Brinellvägen 8, Stockholm, Sverige. Avhandlingen försvaras på engelska. Fakultetsopponent: Prof. Mehran Mostafavi, Université Paris-Sud, Orsay Cedex, Frankrike.

“Success is going from failure to failure
without losing your enthusiasm”

Winston Churchill

Abstract

The process of radiation induced corrosion of copper is not well understood. The most obvious situation where the knowledge of this process is crucial is in a deep repository for high level spent nuclear fuel where the fuel will be sealed inside copper canisters. The radiation will penetrate the canisters and be absorbed by the surrounding environment. In this study gamma irradiations of polished and pre-oxidized copper cubes in anoxic pure water, air of 60-100 % RH and in humid argon were performed. The copper surfaces were examined using IRAS, XPS, cathodic reduction, SEM, AFM, and Raman spectroscopy. The concentration of copper in the reaction solutions was measured using ICP-OES. Also the formation of oxidative species caused by radiation absorption of water was studied by numerical simulations using MAKSIMA software. The corrosion of copper during gamma irradiation vastly exceeds what is expected. The production of oxidative species caused by radiation absorption of water is hundreds of times too low to explain the amount of oxidized copper. A possible explanation for this mismatch is an enhanced radiation chemical yield of $HO^{\cdot}$ on the copper surface. Another explanation is an increased surface area due to oxidation of copper. One speculation is that $HO^{\cdot}$ interacting with the copper oxide can cause oxidation of the metal. If the thermodynamic driving force is large enough then electrons can be conducted from the metal through the oxide to the oxidant. A dramatic increase in surface area together with an increased interfacial yield of $HO^{\cdot}$ might explain the radiation enhanced corrosion process.

Sammanfattning

Strålningsinducerad korrosion av koppar är en process somännu inte är väl utredd. Ett exempel där förståelsen för den här processen är av största vikt, är i ett framtida geologiskt djupförvar av använt högaktivt kärnbränsle där det radiokativa bränslet ska förseglas i kopparkapslar. Gammastrålningen som avges från bränslet kommer passera igenom kapslarna och absorberas av omgivningen. Studier av strålningsinducerade processer i fasgränsytor mellan metalloxider och lösningar har visat att bildandet av vissa radiolysprodukter såsom, H_2, H_2O_2, $HO\cdot$ och e^-, är högre än förväntat precis vid ytan av det fasta materialet. Gammabestrålning av polerad- och föroxiderad koppar i syrefritt vatten, luft med 60-100 % relativ fuktighet samt i vattenmättad argon har utförts. Efter bestrålning undersöktes kopparytorna med IRAS, XPS, katodisk reduktion, SEM, AFM och Raman spektroskopi. Koncentrationen av koppar i reaktionslösningen undersöktes med ICP-OES. Produktionen av oxidanter ifrån gammaradiolys av vatten beräknades med hjälp av mjukvaran MAKSIMA. Korrosionen av koppar under gammabestrålning överstiger kraftigt det förväntade. Produktionen av oxidanter ifrån gammaradiolys är flera hundra gånger för låg för att kunna förklara mängden oxiderad koppar. En möjlig förklaring är en förhöjd produktion av $HO\cdot$ vid kopparytan, en annan förklaring är en kraftigt ökad ytarea från oxidation av koppar. Genom interaktion av $HO\cdot$ med oxiden kan metallen oxideras. Kopparoxid skulle kunna leda elektroner från metallen till oxidanten om oxidanten har tillräcklig oxidationskraft.

List of papers

I. Björkbacka, Å.; Hosseinpour, S.; Leygraf, C.; Jonsson, M. Radiation Induced Corrosion of Copper in Anoxic Aqueous Solution. *Electrochemical and Solid-State Letters* **2012,** *15* (5), C5-C7.

II. Björkbacka, Å.; Hosseinpour, S.; Johnson, M.; Leygraf, C.; Jonsson, M. Radiation induced corrosion of copper for spent nuclear fuel storage. *Radiation Physics and Chemistry* **2013,** *92* (0), 80-86.

III. Björkbacka, Å.; Yang, M.; Gasparrini, C.; Leygraf, C.; Jonsson, M. Kinetics and Mechanisms of Reactions between H_2O_2 and Copper and Copper Oxides. *Dalton Transactions* **2015,** 44, 16045-16051.

IV. Björkbacka, Å.; Johnson, M.; Leygraf, C.; Jonsson, M. The role of the oxide layer in radiation induced corrosion of copper in anoxic water. Manuscript.

V. Björkbacka, Å.; Johnson, M.; Johansson, B.; Ruthland, M.; Leygraf, C.; Jonsson, M. Radiation induced corrosion of copper in humid air and argon. Manuscript.

Contribution to papers

I. Principal author. Planned and performed the experimental work, except IRAS-, AFM- and Confocal Raman-analyses. Major part in writing.

II. Principal author. Planned and performed the numerical simulations and the experimental work, except IRAS-, XPS- and cathodic reduction-analyses. Major part in writing.

III. Principal author. Planned the experimental work. Performed the kinetics part of the experimental work. Major part in writing.

IV. Principal author. Planned and performed the experimental work, except IRAS-analyses. Major part in writing.

V. Principal author. Planned and performed the experimental work, except IRAS- and AFM-analyses. Major part in writing.

Table of contents

1. Introduction

Nuclear power plants in 30 countries are generating 11 % of the world's electricity today. There are 440 commercially operating reactors, 250 research reactors and 180 reactors powering ships and submarines. The nuclear energy production generates almost no emission of greenhouse gasses but do generate highly radioactive waste.[1] The radioactivity of the fuel material will reach natural levels after approximately 100 000 years and during this time it must be isolated from the biosphere.[2] Geological disposal of spent nuclear fuel is being considered the main method for long term storage of high level spent nuclear fuel by many countries.[1]

1.1 Repository for spent nuclear fuel in Sweden

The most developed method today is the Swedish KBS-3 multi-barrier deep geological repository concept, which is planned to be used in Finland and in Sweden.[3] According to this concept, copper canisters with cast iron inserts containing spent nuclear fuel elements will be deposited at 500 meters depth in ground water saturated granitic bedrock, see Figure 1.[2] The canisters will be deposited individually in vertical bore holes drilled in the floor of a tunnel system. After deposition the canisters will be embedded in compacted bentonite clay and the tunnels will be sealed with bentonite backfill, see Figure 2.[3] The engineered barriers in the deep repository will consist of naturally occurring materials.

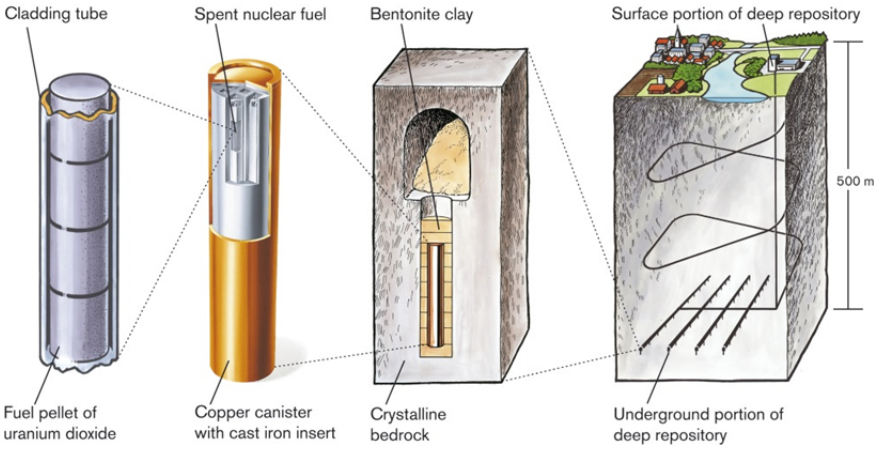

Fig 1. The KBS-3 multi-barrier deep geological repository concept. © SKB AB

The copper will provide corrosion resistance to the canisters and the bentonite clay will absorb groundwater and protect the canister from movements in the bedrock. The bedrock itself will act as the last barrier as it is mechanically, thermally and chemically stable.[2]

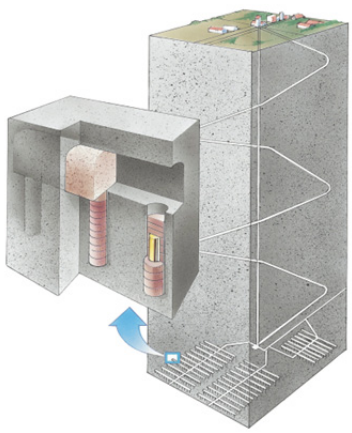

Fig 2. Emplacement of a canister in compacted bentonite clay with bentonite backfill in the KBS-3 concept. © SKB AB

1.2 The copper canister

The purpose of the copper canister is to isolate the spent nuclear fuel from the biosphere until the radioactivity of the fuel material has reached natural levels, approximately after 100 000 years. The maximum allowed temperature of the canister surface is set to 100°C and the maximum allowed radiation dose rate on the canister surface is set to 1 $Gy \cdot h^{-1}$ (1 Gy = 1 $J \cdot kg^{-1}$).[3] These requirements must be fulfilled in the design of the canisters.

1.2.1 Design of the copper canister

The cast iron inserts will provide radiation shielding and mechanical strength to the canisters to withstand the loads at disposal depths around 500 meters. Steel channels in the insert will keep the spent nuclear fuel elements in place. Depending on the type of fuel that will be encapsulated there will be either 4 (PWR-type insert) or 10 (BWR-type insert) steel channels.[4] The copper is chosen for its resistance to the chemical environment prevailing in a future deep geological repository. To prevent corrosion damage of the canisters the thickness of the copper shell has been set to 50 mm. The height of the copper shell will be 4.835 meters and the outer radius will be 0.525 meters.[5] The weight of the copper shell will be 7500 kg and the total weight of a canister (spent fuel elements included) will be 24600-26800 kg,[4] depending on the fuel type. A canister with an insert for BWR-type spent fuel can be seen in Figure 3.[3]

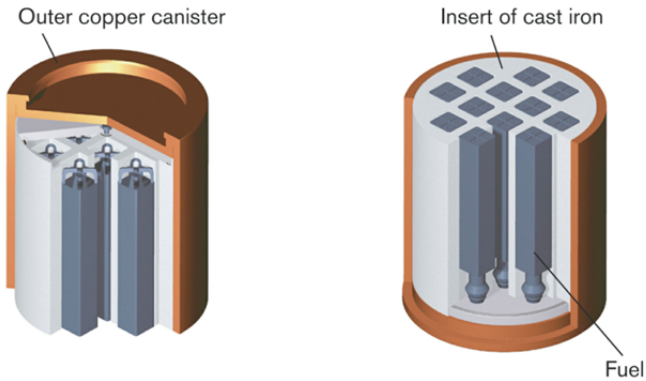

Fig 3. A BWR-type spent nuclear fuel canister, both the cast iron insert and the outer copper shell is shown. © SKB AB

1.2.2 From manufacturing to deposition

Before deposition in the deep repository the copper canisters will be exposed to different media that will initiate atmospheric corrosion. After manufacturing the canisters will first be transported to the encapsulation plant located near the interim storage for high level spent nuclear fuel. There, the fuel assemblies will be encapsulated inside the canisters before sealing them by friction stir welding. The fuel assemblies are selected due to their burnup and age to prevent dose rates of above 1 $Gy \cdot h^{-1}$ on the outer canister surface. The assemblies are dried before they are encapsulated to reduce the amount of water inside the canisters. The maximum allowed water content is 600 g. Before the mounting of the copper lids onto the canisters the atmosphere inside is replaced by argon to at least 90 %.[6] The canisters are then placed in transportation casks which are either moved to a parking bay or directly to the harbor from where the canisters will be

transported by boat to the deep repository. After arrival to the location of the deep repository the canisters are inspected and parked in a parking bay until deposition.[4] The procedure is summarized in Figure 4.

1.2.3 Initial state of the canister

Initially in the deep repository there will be air trapped in the bentonite clay and the backfill surrounding the canisters. Depending on the volumes and porosity of the buffer and backfill the amount of trapped oxygen per canister is approximately 475 moles. However, due to slow diffusion, oxygen consumption by reactions with accessory minerals and by microbial activity, only a small part is expected to reach the canister.[5] The bentonite clay surrounding the copper canisters will be 85 % water saturated at deposition in the repository.[7] It is estimated that complete water saturation will take approximately fifteen years and anoxic conditions are likely to be reached right after.[2]

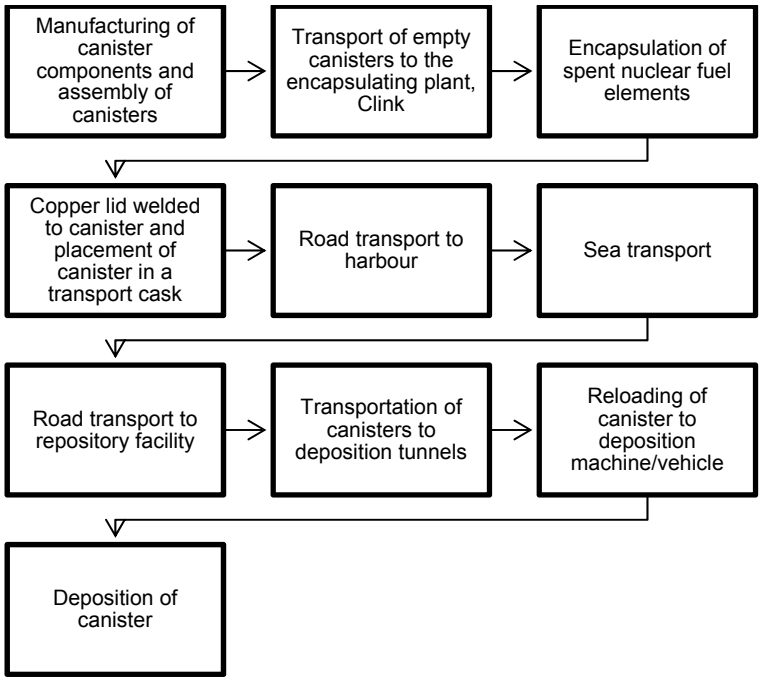

Fig 4. Canister pathway from production to deposition.

1.3 Atmospheric corrosion of copper

When copper is exposed to the outdoor atmosphere water in the air will adsorb on to the metal surface. Depending on actual exposure conditions it may take a few hours to reach steady state at a constant relative humidity (RH). The water film, with a thickness depending on the RH of the air, can act as an electrolyte and a corrosion process can be initiated. At 30 °C in 60 % and 90 % RH the adsorbed water films consists of approximately 8 and 18 monolayers respectively.[8, 9] At 100 % RH the numbers of monolayers are no longer meaningful to measure as they increase continuously due to condensation of the moisture. The main

corrosion product formed during atmospheric corrosion of copper is cuprite (Cu_2O) and it is always the corrosion product in contact with the copper surface.[10] Depending on the pH of the adsorbed water film both the formation and solubility of the corrosion film changes. At pH 5 a thick and porous corrosion layer consisting of cubic Cu_2O crystals forms on the copper surface while at pH 10 the formed corrosion film is thin, dense and protective.[11] The solubilities of crystalline Cu_2O in water at pH 5 and 6 are 1 – 10 μM respectively.[12] Nitric acid (HNO_3) can be formed from pollutants in air. When copper is exposed to HNO_3 at 65 % RH and 25 °C the main corrosion products are Cu_2O and gerhardtite ($Cu_4(NO_3)_2(OH)_6$).[13]

1.4 Radiation chemistry

The amount of radiation energy absorbed per mass unit is recognized as absorbed dose (D). The SI unit for absorbed dose is Gray (Gy) and it is defined as 1 Gy = 1 $J \cdot kg^{-1}$. The dose rate is the absorbed dose per time ($Gy \cdot s^{-1}$). The consequences of absorbing radiation energy depend on the radiation source and the absorbing material. For example little influence is caused by gamma irradiation of metals while irradiation by heavy particles causes displacements in the metal lattice. When gamma radiation is absorbed by water, instead ionizations and excitations of the water molecules occur. The radiation chemical yield, or the G-value (G(x)), is described as the number of molecules of a product or reactant, (x), formed or consumed per Joule absorbed radiation energy. The G-value ($mol \cdot J^{-1}$) is expressed as in Equation 1:

$$G(x) = \frac{n_x}{\partial E} \quad (1)$$

where G(x) is the radiation chemical yield for a certain product (x), n_x is the number of moles of x formed per absorbed energy unit (δE) (J). The G-value together with the dose rate and the density of the irradiated medium can be used to determine the rate of formation ($mol \cdot dm^{-3} \cdot s^{-1}$) of a certain radiolysis product.[14]

1.4.1 Gamma radiolysis

Radiolysis of water occurs when water absorbs radiation. H_2O^+ is formed through ionization and will react further with H_2O and form $HO\cdot$ and H_3O^+. H_2O^* dissociates into H_2, $O\cdot$, $H\cdot$ and $HO\cdot$. Recombination reactions form molecular and secondary radical products for example hydrogen peroxide (H_2O_2). In Figure 5, the time scale of events during the radiolysis of neutral water is shown. The G-values for the radiolysis products formed in pure water under gamma irradiation are well established and they are given in Table 1.[15]

Table 1. Product yields (G-values) ($\mu mol \cdot J^{-1}$) in gamma irradiated neutral water.

$G(-H_2O)$	$G(H_2)$	$G(H_2O_2)$	$G(e^-_{aq})$	$G(H\cdot)$	$G(HO_2\cdot)$	$G(HO\cdot)$	$G(H_3O^+)$
0.430	0.047	0.073	0.280	0.062	0.0027	0.280	0.280

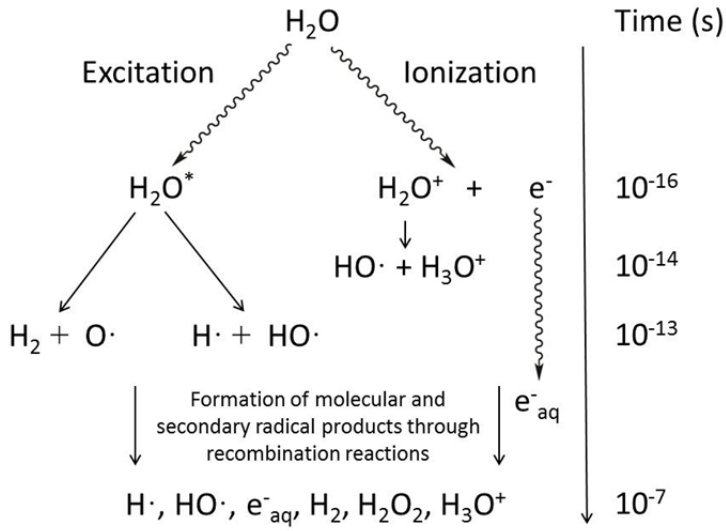

Fig 5. Time scale for the radiolysis of neutral water.

Radiolysis of humid air results in the production of HNO_3.[15] In radiolysis of saline aqueous solutions the $HO\cdot$ reacts with Cl^- to form of $HClO^-$ which can react further with H^+ to form $Cl\cdot$.[14]

1.4.2 Radiation chemistry in heterogeneous systems

Homogeneous radiolysis of pure water is well established and the radiation chemical yields are generally accepted. The aqueous radiation chemistry at solid surfaces on the other hand is still not well understood and it can be very different from that in bulk water. It is practically very difficult to study the radiation induced processes occurring at solid-liquid interfaces. Important parameters that needs to be understood are the dose distribution in a heterogeneous system, kinetics and mechanisms for reactions

between radiolysis products in solution at the solid surface, adsorption, dissolution and effects of energy absorption by the solid material.[16] Several earlier studies have confirmed an increase in the radiation chemical yield of hydrogen ($G(H_2)$) in water-metal oxide systems of high solid surface-area-to-solution-volume ratios.[17-21] The exact mechanism for this surface enhanced production is still unknown but an excess of electrons in the water phase has been observed.

At low solid surface-area-to-solution-volume ratios the surface reactions will not influence the concentration of radiolysis products in the bulk and the heterogeneous system should behave more like a homogeneous system in terms of concentrations of aqueous radiolysis products. It has been shown that in such systems numerical simulations of homogeneous water radiolysis can be used to calculate the concentration of radiolysis products in the system.[22] This study showed that the dissolution of pure uranium dioxide powder (UO_2) in anoxic water under continuous gamma irradiation could be estimated in excellent agreement with experimental results. In this particular case, corrosion of the uranium dioxide powder was shown to be completely governed by the aqueous radiation chemistry. The rate of oxidation at a given time during irradiation is calculated from the oxidant concentrations at that given time using Equation 2.

$$Rate = \frac{dn_S}{dt} = A_S \sum_{ox=1}^{n} k_{ox} [Ox] \frac{n_{e^-}}{2} \qquad (2)$$

In Equation 2, A_S is the solid surface area (m^2), k_{ox} is the rate constant for the reaction between a given oxidant and the solid

surface ($m \cdot s^{-1}$), $[Ox]$ is the time dependent concentration of a given oxidant ($mol \cdot m^{-3}$) and n_e- is the number of electrons involved in the redox process.[16] To calculate the total amount of oxidized solid, Equation 2 must be integrated over time taking the concentration time dependence into account.

1.4.3 Corrosive radiolysis products on the copper canister surface

Two oxidants, H_2O_2 and $HO\cdot$, from aqueous gamma radiolysis have significantly higher standard reduction potentials ($E^\circ(H_2O_2/2H_2O)$=1.77 V and $E^\circ(HO\cdot_{aq}/H_2O)$=2.59 V) than copper ($E^\circ(Cu^+/Cu(s))$=0.520 V or $E^\circ(Cu^{2+}/Cu(s))$=0.341 V) and are therefore able to corrode copper.[23-25] If gamma radiation is instead absorbed by humid air, HNO_3 which is also able to oxidize copper,[13] is formed.[14]

1.4.4 Reactions between H_2O_2 and metal oxides

The most important oxidant in radiation induced dissolution of UO_2-based nuclear fuel has been identified as H_2O_2 and for this reason it has been studied quite extensively in recent years.[22, 26-29] It has been shown that H_2O_2 can react with metal oxides in two different ways; by catalytic decomposition and by electron-transfer.[30, 31] The catalytic decomposition consumes H_2O_2 but leaves the oxide in its original state while the electron-transfer leads to corrosion. The mechanism for catalytic decomposition of H_2O_2 on a surface is summarized in Equations 3-5 ((ads) represents a surface adsorbed state):[28, 30]

$$H_2O_2\,(ads) \rightarrow 2\ HO\cdot\ (ads) \quad (3)$$

$$H_2O_2\,(ads) + HO\cdot\ (ads) \rightarrow H_2O\ (ads) + HO_2\cdot\ (ads) \quad (4)$$

$$2\ HO_2\cdot\ (ads) \rightarrow H_2O_2 + O_2 \quad (5)$$

To confirm the formation of surface bound HO· a radical scavenger, such as methanol (CH_3OH),[32-34] must be used since it is not possible to detect HO· directly due to its very high reactivity. The main product from the reaction between CH_3OH and HO· is the hydroxymethyl radical ($\cdot CH_2OH$) which accounts for approximately 93% of the products.[35] In deoxygenated solution $\cdot CH_2OH$ reacts further, to form mainly ethylene glycol $(CH_2OH)_2$ and formaldehyde (CH_2O), via disproportionation.[36, 37] CH_2O can be detected via a modified version of the Hantzsch method.[38] There are several possible reaction pathways for $\cdot CH_2OH$ with metal and metal ions to further form CH_2O and therefore the yield of CH_2O obtained must be considered a relative measurement of HO·.[39-41]
An experimental study of the reaction between CH_3OH and HO·, initiated by gamma irradiation of anoxic CH_3OH-solution, confirmed the formation of CH_2O. The yield was found to be quite low, only 14%.[34]

1.5 Previous work on radiation induced corrosion of copper

Despite the importance of understanding the process behind the radiation induced corrosion of copper, relatively few previous studies on this topic have been reported. Some studies indicate the occurrence of radiation induced copper corrosion while other studies indicate no such effect.

Electrochemical studies of the influence of gamma radiation on copper have been performed in saline solutions with different outcome.[42-44] In two cases using total doses of 1.4 kGy, in temperatures of 30 and 150 °C under anoxic conditions no corrosion effects could be seen compared to unirradiated reference cases. In the third case, using a total dose of 13.6 kGy, in room temperature under oxic conditions, a significantly higher corrosion rate was observed in the presence of gamma irradiation than without. Studies of gamma radiation induced corrosion of copper in moist air have also been performed. Using total doses of 107 - 510 kGy, RH of 40 - 100 % and temperatures of 90 - 150 °C, both Cu_2O and tenorite (CuO) could be detected on the copper surfaces.[45, 46] Radiation experiments on copper under oxic conditions in water at 42 °C and groundwater at 95 °C using total doses of 720 – 5 016 kGy resulted in pitting corrosion[47] and corrosion rates 30 times higher than in similar experiments without radiation.[48] The differences in experimental conditions between these studies, i.e. several oxic/anoxic solution compositions exposed to dose rates and total doses which vary by several orders of magnitude, makes it impossible to draw meaningful conclusions.

1.6 Objectives

The aim of this work is to elucidate the mechanisms and dynamics of radiation induced corrosion of copper in aqueous environments since, despite its importance, fairly few systematic studies on this topic are reported.

The main reason for studying this system is the soon-to-be-built deep geological repository for high level spent nuclear fuel in Finland and in Sweden. Beside this reason an increased understanding of the radiation induced processes occurring at solid-liquid interfaces is desirable.

2. Experimental details

For all solutions water from a Millipore Milli-Q system (18.2 $M\Omega \cdot cm^{-1}$) of pH 5.5 was used. All H_2O_2-solutions were prepared from a 30 % standard solution (CAS [7722-84-1], Merck). All experiments were performed at ambient temperature (19-22 °C). All powder samples were weighted on a Mettler Toledo AT261 Delta Range Microbalance. All aqueous particle suspensions were stirred using a magnetic stirrer at 750 rpm and purged with N_2 (Strandmøllen AB, purity of 99.999%) for at least 30 minutes prior to the experiments.

All anoxic samples were prepared in an Ar filled (Strandmøllen AB, purity of 99.995 %) glovebox and all oxic samples were prepared in indoor air with a RH of approximately 60 %. All reaction vessels were covered with aluminum foil to avoid absorption of UV-light. The pH was measured using a 713 pH Meter from Metrohm or pH-paper from Merck.

2.1 Materials

Copper cubes, originating from a SKB copper canister wall, (99.992% Cu, major impurities are P and Ag) of the sizes 10×10×10 mm were grinded on all sides with SiC abrasive papers of 1200 grit. One side was further polished with 3 μm polycrystalline diamond paste (Struers). All polishing steps were made in 99.5% ethanol. After polishing, the copper pieces were sonicated in 99.5 % ethanol for five minutes and then dried under N_2 (AGA Gas AB, purity of 99.996%) in a glovebox.

All experiments were performed with at least two separate pieces

of copper simultaneously. A reference sample, not irradiated but otherwise treated the exact same way as the irradiated samples, was also included in every experiment.

Cu-powder (CAS [7440-50-8], spherical, -100/+325 mesh, 99,9 %, Alfa Aesar), copper(I)oxide (Cu_2O), (CAS [1317-39-1], powder, anhydrous, 99,9 %, Sigma-Aldrich), copper(II)oxide (CuO): (CAS [1317-38-0], powder, 99,99 %, Aldrich) were used without further purification. The B.E.T surface areas of the three different powders were: Cu-powder (0.1 $m^2 \cdot g^{-1}$); Cu_2O (0.5 $m^2 \cdot g^{-1}$); CuO (17.9 $m^2 \cdot g^{-1}$).

2.2 Kinetic study

The concentration of H_2O_2 as a function of time was determined using the Ghormley triiodide method. In this method, I^- is oxidized to I_3^- by H_2O_2. The absorbance of the product I_3^- was measured spectrophotometrically at a wavelength of 355 nm. There is a linear correlation between the absorbance of I_3^- and the H_2O_2 concentration [27]. An extracted sample volume of 0.2 ml was filtered through a Gema Medical Cellulose Acetate syringe filter 0.2 μm/13 mm and further used for the measurement of the H_2O_2 concentration. The pH of the oxide suspensions was approximately 6 before, during and after the reactions. The initial experimental conditions for the reactions between H_2O_2 and powders were 50 ml 0.5 mM of H_2O_2 and the amounts of powders were varied between 0.007 and 1.5 g. Two sets of experimental conditions were used for the study of the reactions between H_2O_2 and Cu-cubes. Initial experimental conditions were 50 ml 0.5 mM of H_2O_2 and 100 mM of CH_3OH in 100 ml 5 mM of H_2O_2. No change in absorbance was

spectrophotometrically detected for possible background reactions between copper and $H_2O/CH_3OH/ CH_2O$.

2.3 Mechanistic study

The reaction between CH_3OH (HPLC grade CH_3OH, (CAS [67-56-1]), Aldrich, 99,9 %) and HO· producing CH_2O [34] was monitored using a modified version of the Hantzsch reaction to quantify the amount of CH_2O.[38] The CH_2O reacts further with Acetoacetanilide AAA (CAS[102-01-2], Alfa Aeser, 98%) and Ammonium acetate (CAS[631-61-8], 98 %, Lancaster) to form a dihydropyridine derivative with maximum absorbance wavelength at 368 nm. An extracted sample volume of 1.5 ml was filtered through a Gema Medical Cellulose Acetate syringe filter 0.2 μm/13 mm and further used for the measurement of the CH_2O concentration. The initial experimental conditions for the reactions between H_2O_2 and powders were 100 mM of CH_3OH in 50 ml 5 mM of H_2O_2 and the amounts of powders were varied between 0.0125 and 3 g. The initial experimental conditions for the reactions between H_2O_2 and Cu-cubes were 100 mM of CH_3OH in 100 ml 5 mM of H_2O_2. No change in absorbance was spectrophotometrically detected for possible background reactions between copper and $H_2O/CH_3OH/ CH_2O$.

2.4 Numerical simulations

Numerical simulations of homogeneous radiation chemistry of water were performed using the software MAKSIMA-chemist.[49] The radiation chemical yields, G-values, for the water radiolysis

products used in the simulations are presented in Table 1. The reactions and corresponding rate constants are presented in Table 2.[50]

Table 2. Reaction scheme used in the MAKSIMA simulations.

Reactions	Rate constants ($M^{-1}\cdot s^{-1}$)
$HO\cdot + HO\cdot = H_2O_2$	4.0×10^{9}
$HO\cdot + e^- = HO^- + H_2O$	2.0×10^{10}
$HO\cdot + H\cdot = H_2O$	2.5×10^{10}
$HO\cdot + O_2^- = HO^- + O_2$	1.0×10^{10}
$HO\cdot + H_2O_2 = H_2O + O_2^- + H^+$	2.3×10^{7}
$HO\cdot + H_2 = H_2O + H\cdot$	4.0×10^{7}
$e^- + e^- = HO^- + HO^- + H_2$	5.0×10^{9}
$e^- + H\cdot = HO^- + H_2$	2.0×10^{10}
$e^- + HO_2\cdot = HO_2^- + H_2O$	2.0×10^{10}
$e^- + O_2^- = HO_2^- + HO^-$	1.2×10^{10}
$e^- + H_2O_2 = HO\cdot + HO^- + H_2O$	1.6×10^{10}
$e^- + H^+ = H\cdot + H_2O$	2.2×10^{10}
$e^- + O_2 = O_2^- + H_2O$	2.0×10^{10}
$e^- + H_2O = H\cdot + HO^- + H_2O$	2.0×10^{1}
$H\cdot + H\cdot = H_2$	1.0×10^{10}
$H\cdot + HO_2\cdot = H_2O_2$	2.0×10^{10}
$H\cdot + O_2^- = HO_2^-$	2.0×10^{10}
$H\cdot + H_2O_2 = HO\cdot + H_2O$	6.0×10^{7}
$H\cdot + HO^- = e^-$	2.0×10^{7}
$H\cdot + O_2 = O_2^- + H^+$	2.0×10^{10}
$HO_2\cdot^+ = O_2^- + H^+$	8.0×10^{5}
$HO_2\cdot + HO_2\cdot = O_2 + H_2O_2$	7.5×10^{5}
$HO_2\cdot + O_2^- = O_2 + HO_2^-$	8.5×10^{7}
$O_2^- + H^+ = HO_2\cdot$	5.0×10^{10}
$H_2O_2 + HO^- = HO_2^- + H_2O$	5.0×10^{8}
$HO_2^- + H_2O = H_2O_2 + HO^-$	5.7×10^{4}

2.5 Instrumentation

Gamma irradiations were performed using a MDS Nordion 1000 Elite Cs-137 gamma source. The dose rates employed varied between 0.02 and 0.3 $Gy \cdot s^{-1}$ depending on shielding and the position of the samples inside the gamma source. The dose rates were determined using Fricke dosimetry.[51]

UV/vis spectra were collected using a WPA Biowave II or a Jasco V-630 UV/vis spectrophotometer.

Trace elemental analysis was performed on all solutions using inductively coupled plasma optic emission spectroscopy (Thermo Scientific iCAP 6000 series ICP spectrometer (ICP-OES)). The analysis for copper was performed at wavelengths of 219.9 and 217.8 nm using ICP multi element standard IV from Merck. Filtrations were performed using filters from Gema Medical (0.2 µm) and from Whatman (0.02 µm).

Surface characterization of the polished sides of the copper cubes was performed using a Digilab FTS 40 Pro infrared reflection absorption spectrometer (IRAS) with P-polarized light with an incident angle of 78° using 512 or 1024 scans with a resolution of 4 cm^{-1}. As background sample an unirradiated polished copper cube was used.

XPS spectra were recorded with a Kratos Axis Ultra electron spectrometer with a delay line detector. A monochromated Al K_α

source operated at 150 W, a hybrid lens system with a magnetic lens, providing an analyzed area of 0.3×0.7 $(mm)^2$, and a charge neutralizer were used for the measurements. The base pressure in the analysis chamber is below $3 \cdot 10^{-9}$ Torr. The binding energy (BE) scale was referenced to the C 1s of aliphatic carbon, set at 285.0 eV. Processing of the spectra was accomplished with Kratos software using Gaussian and Lorenzian functions in ratio of about 70% to 30%. Shirley background subtraction is applied. The depth of analysis for metal oxides/hydroxides is about 6 nm. The element detection limit is typically 0.1 atomic %.

Surface examinations were performed using a FEG-SEM Zeiss Sigma VP with a Gemini field emission column scanning electron microscope or a Jeol JSM-6490LV scanning electron microscope with a Jeol EX-230 energy dispersive X-ray spectrometer.

Nitrogen adsorption–desorption isotherms were recorded at liquid nitrogen temperature (77 K) for all powders using a Micromeritics ASAP2020 volumetric adsorption analyser. The samples were treated under near-vacuum conditions (< 10^{-5} Torr) at a temperature of 300°C for 10 h. The specific surface areas of the materials were calculated from the recorded data according to the B.E.T. isotherm in the range of relative pressures of 0.05 - 0.15. The total pore volume was calculated at a relative pressure of 0.99.

Surface topography was obtained using an Agilent 5500 atomic force microscope (AFM) in static mode with a commercially obtained cantilever or a Bruker Dimension Icon (Bruker®, Santa

Barbara, CA) AFM operating in standard tapping mode in air. Silicon tips, RTESPA (Veeco) were cleaned in UV chamber for 20 min, rinsed with ethanol (99,6%) and dried with nitrogen gas prior to use. The surface height profiles of the scanned areas were then obtained using the line scan on the created AFM image.

Cathodic reductions were conducted following the procedure in ASTM B825-13,[52] using an EG &G Princeton Applied Research potentiostat/galvanostat model 263A to quantify the amount of oxide formed on the copper samples. 0.1 M KCl was used as the electrolyte solution with a SCE reference electrode and a platinum counter electrode. The cathodic current density was 0.05 $mA \cdot cm^{-2}$. To perform the experiments in oxygen-free electrolyte, the solution was purged with N_2 (AGA Gas AB, purity of 99.996 %) 30 min prior to the experiment. The correlated time for the point of hydrogen evolution was used to provide the amount of electrons needed to reduce the oxidized copper back to metallic copper. If the composition of the oxide layer is known, then, according to Faraday's law, the equivalent thickness of the oxide formed on the surface can be obtained using Equation 6.

$$d = (t \times I \times M)/(A \times n \times \rho \times F) \qquad (6)$$

In Equation 6, d is the oxide thickness (m), t is the time required to reduce the oxide (s), I is the applied current (A), M is the molar mass of the oxide ($g \cdot mol^{-1}$), A is the sample area in contact with the electrolyte (m^2), n is the number of electrons required to reduce a unit of molecular weight of oxide, ρ is the specific weight of the

reduced oxide ($g \cdot m^{-3}$), and F is Faraday's constant (9.65×10^4 $C \cdot mol^{-1}$). The densities used for calculations of the oxide thickness for CuO and Cu_2O are 6.315 and 6 $g \cdot (cm^3)^{-1}$ respectively.[53]

Confocal Raman imaging was performed on a 40 × 40 μm area of the irradiated sample using a WITEC alpha 300 system Confocal Raman Microscope equipped with a 532 nm laser source and a 50 X Nikon objective.

A Memmert oven was used for pre-oxidation of copper cubes in 90°C for 24 h under unlimited amount of air.

3. Results and discussion

3.1 Gamma radiation experiments

Copper cubes were irradiated under different conditions by gamma radiation. Duplicates were made in each irradiation experiment as well as a reference sample. The reference sample was treated under the same conditions as the irradiated samples with the exception of exposure to gamma radiation.

3.1.1 Polished copper cubes in anoxic water

Polished copper cubes were irradiated in 10 ml of anoxic pure water for 2-168 hours. The dose rates varied between 0.02 and 0.3 $Gy \cdot s^{-1}$ and the maximum total dose absorbed was 95 kGy. Already by visual inspection it is obvious that the irradiated copper samples are more corroded than the reference samples.

3.1.1.1 Measured concentration of copper in solution after irradiation of polished copper cubes

A series of gamma radiation exposures were performed to study the effect of the absorbed total dose on the corrosion behavior of polished copper in anoxic pure water. When measuring the concentration of copper in solution using ICP-OES, the radiation enhanced corrosion is detected already at very low total doses of 1.5 kGy. At absorbed total doses of 0.75-1.5 kGy no detectible difference was found between irradiated and unirradiated copper samples. Both for irradiated (total doses up to 1.5 kGy) and unirradiated samples, the copper concentration in solution was approximately 2 μM. When increasing the absorbed total dose

gradually up to 74 kGy there is a significant difference in concentration of copper in solution between irradiated and unirradiated copper samples. When comparing the three different dose rates in terms of copper release to the aqueous solution, it can be concluded that the concentration of copper varies depending on the dose rate used. The results are presented in Figure 6 together with photographs of copper cubes exposed to different total doses. It is quite clear that the two copper cubes exposed to the two highest total doses are more corroded than the one exposed to the lowest total dose. The concentration of copper in solution is increasing with increasing absorbed total dose. [54]

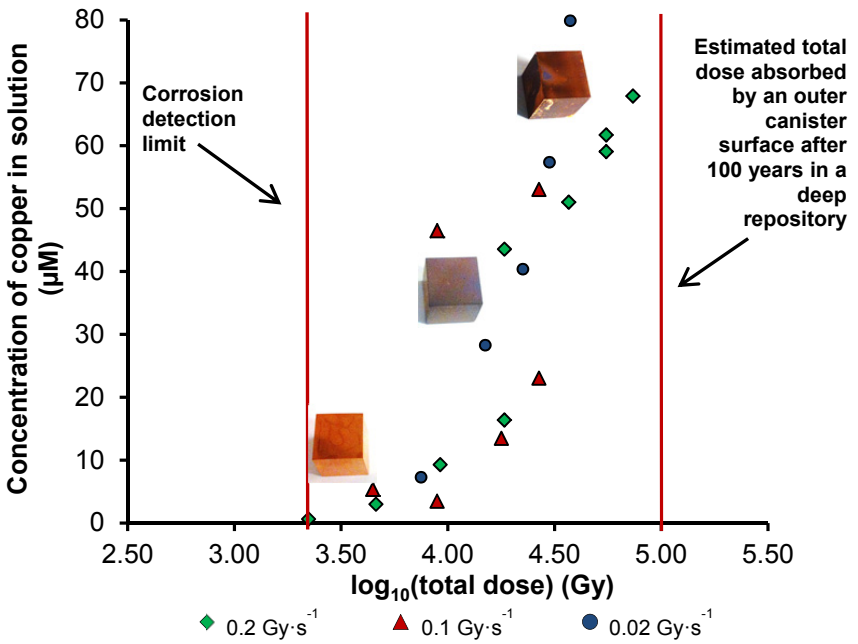

Fig 6. Measured concentrations of copper (µM) in aqueous solution as a function of absorbed total dose (Gy). Corrections for the unirradiated reference samples are made. © Elsevier B.V.

There is a statistically significant difference in the yield of copper in solution, between the dose rates of 0.02 and 0.2 $Gy \cdot s^{-1}$. For the dose rate of 0.2 $Gy \cdot s^{-1}$ the yield of copper in solution is 0.0005 ± 0.0002 $\mu mol \cdot J^{-1}$ while for the dose rate of 0.02 $Gy \cdot s^{-1}$ the yield of copper in solution is 0.0023 ± 0.0002 $\mu mol \cdot J^{-1}$.

3.1.1.2 Oxide formation during irradiation of polished copper cubes

When examining the oxide layer formed during irradiation of copper samples using IRAS, the first sign of radiation enhanced corrosion was detected at higher total doses than when using ICP-OES, approximately at a total dose of 20 kGy. An unirradiated reference sample was used as background in the IRAS examinations. An IRAS spectrum of a copper surface exposed to 26.7 kGy at a dose rate of 0.1 $Gy \cdot s^{-1}$ is shown in Figure 7.

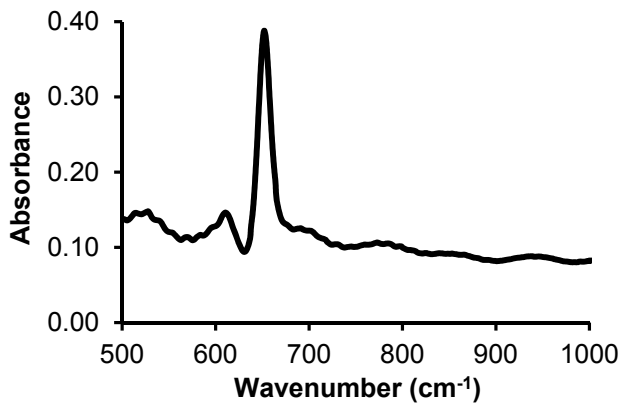

Fig 7. IRAS spectra of an irradiated copper surface. The dose rate was 0.1 $Gy \cdot s^{-1}$ and the total dose absorbed was 26.7 kGy. © Elsevier B.V.

Cu_2O was detected as the main corrosion product on all copper surfaces exposed to total doses higher than 20 kGy.
An obvious Cu_2O peak is seen at ~652 cm^{-1} and at ~610 cm^{-1} a weaker peak is seen which also originates from Cu_2O.[55] Close to the cutoff frequency, CuO has a wide peak at ~520-560 cm^{-1},[56] and as can be seen in Figure 7, it cannot be ruled out that there are low amounts of CuO present on the surface. No other peaks were observed in the scanning range between 500 and 4000 cm^{-1}.[54]

XPS analyses support the results from IRAS examinations. Copper cubes were exposed to anoxic pure water for 96 hours, 1 l of 10 µM of H_2O_2 for 96 hours and gamma radiation for 96 hours absorbing a total dose of 74 kGy. The results show that the copper content in the oxides on all three samples are quite similar, see Table 3 and Figure 8. Larger amounts of Cu(I) compounds were detected together with very small amounts of Cu(II) compounds. The Auger parameter was determined at 1848.9 eV.[57]

Table 3. XPS data from measurements of copper surfaces exposed to anoxic pure H_2O for 96 hours, 1 l of 10 µM of H_2O_2 and gamma irradiation in anoxic pure water at a dose rate of 0.2 $Gy \cdot s^{-1}$ and a total dose of 74 kGy. © Elsevier B.V.

	Reference sample	H_2O_2 exposed sample	Irradiated sample	Chemical binding compound
	AC (at%)	AC (at%)	AC (at%)	
Cu 2p 3/2	24.9	31.2	32.6	Cu (I)
	2.2	1.3	1.8	Cu (II)

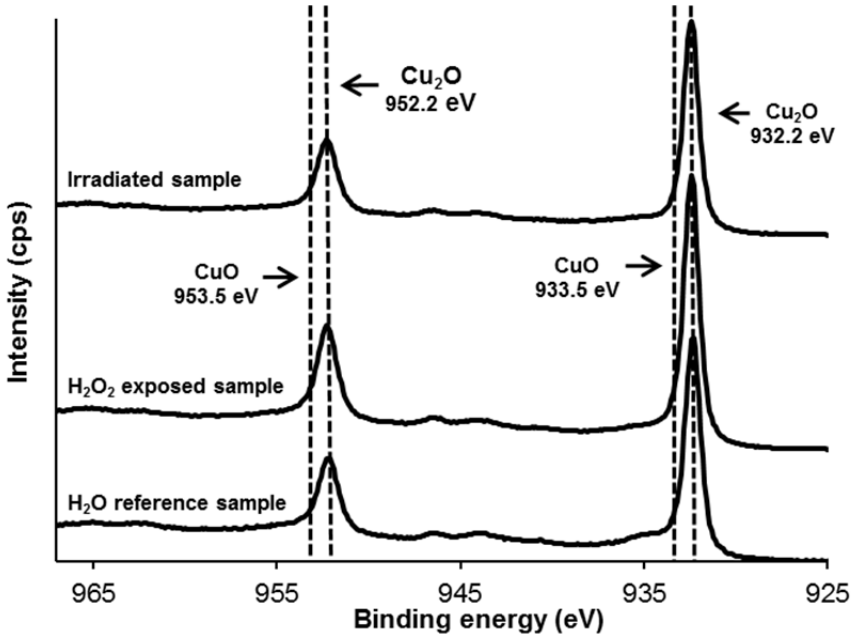

Fig 8. XPS spectra of copper surfaces exposed to anoxic pure H_2O for 96 hours, 1 l of 10 µM of H_2O_2 and gamma irradiation in anoxic pure water at a dose rate of 0.2 $Gy \cdot s^{-1}$ and a total dose of 74 kGy.

In Figure 9, the results from electrochemical measurements, cathodic reductions, are presented. After irradiation of a copper cube, at a dose rate of 0.2 $Gy \cdot s^{-1}$ and a total dose of 74 kGy, the amount of electrons required to reduce the oxidized copper back to metallic copper is 0.52 $\mu mol \cdot cm^{-2}$. On the reference sample, exposed only to anoxic pure water for 96 hours, the amount of electrons required to reduce the oxidized copper back to metallic copper is only 0.07 $\mu mol \cdot cm^{-2}$. Assuming that the oxide layer is pure Cu_2O then the oxide thickness on the surface of the irradiated sample is estimated to approximately 100 nm while the oxide layer

thickness on the surface of the unirradiated reference sample is only 4 nm. The amount of oxidized copper, calculated from the results from cathodic reduction, must be considered as an average value due to the heterogeneity of the oxide layer formed during gamma irradiations.[54] The major part of the oxidized copper, after irradiation at a dose rate of 0.2 $Gy \cdot s^{-1}$ for 96 hours, is situated in the oxide layer while less than 0.5 % is released into solution.

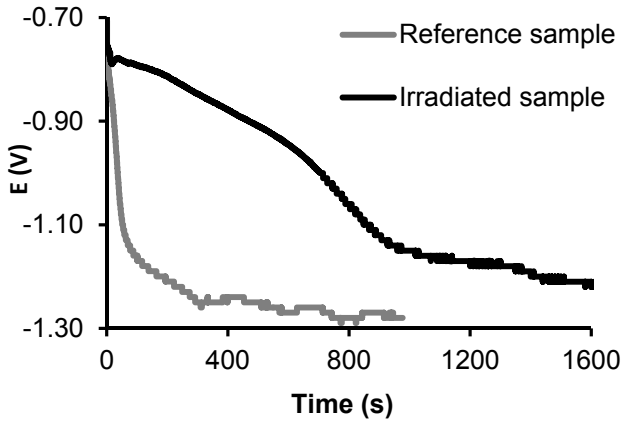

Fig 9. Results from cathodic reduction measurements of an irradiated copper surface and a reference copper surface. © Elsevier B.V.

3.1.1.3 Formation of local corrosion features during irradiation of polished copper cubes

SEM images from surface examinations of reference and irradiated copper surfaces are presented in Figure 10 a, b and c. Examinations of the reference samples reveal a homogeneous surface only with markings from polishing, as can be seen in Figure 10 a. The examinations of irradiated copper samples reveal

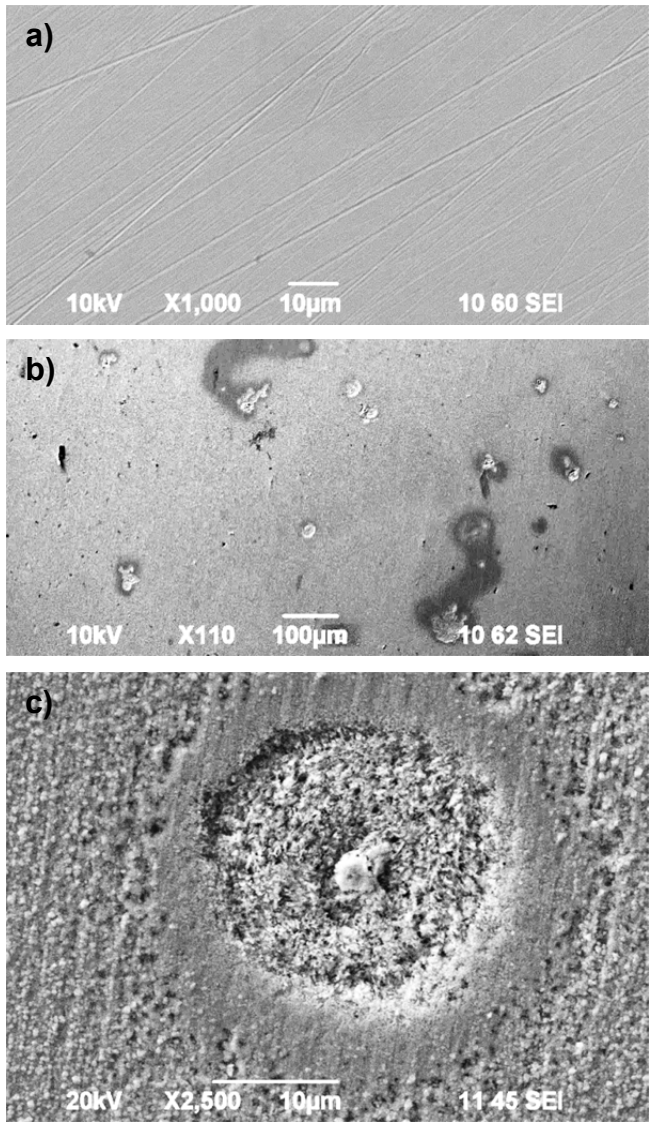

Fig 10 a, b and c. SEM-images of a) a reference copper surface exposed to anoxic pure water for 96 hours , b) an irradiated copper surface using a dose rate of 0.1 $Gy \cdot s^{-1}$ and a total dose of 62 kGy and c) a close-up on one of the local corrosion features.

a crystalline oxide layer with local corrosion features embedded within the oxide. The corrosion features are frequently circular in shape; they are of different sizes and are spread all over the surface, as can be seen in Figure 10 b. In the close-up image of a local corrosion feature in Figure 10 c, it can be seen that the crystalline oxide layer is surrounding a quite flat and ring-shaped surface with a rougher surface in the center.
Neither distribution nor size of the local corrosion features seems to be dependent on the dose rate or the total absorbed dose.[54]

SEM-EDS imaging shows that the oxygen content is higher within the local corrosion features than outside them, see Figure 11.

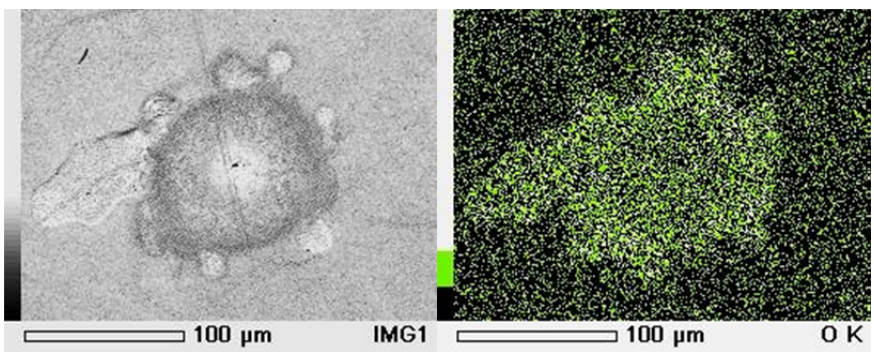

Fig 11. SEM-EDS images of a local corrosion feature where it clearly can be seen that the oxygen content is higher within the feature than outside.

In Figure 12 the result from an AFM measurement of a local corrosion feature is displayed.

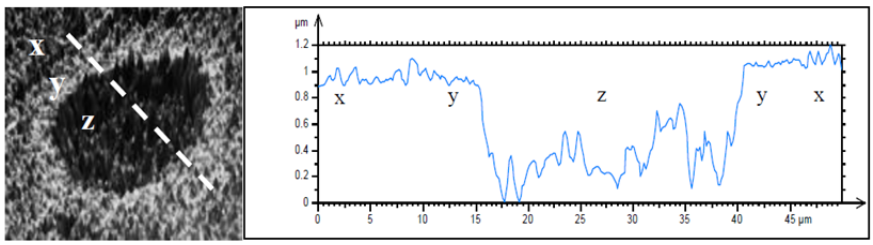

Fig 12. AFM topographic image of a local corrosion feature.

The corrosion feature in the AFM image is divided into three different areas; the crystalline oxide layer, x, the flat ring, y, and the rough center, z. The two outer areas, x and y, have similar heights while the center area, z, is approximately 800 nm deep.[58]

A Confocal Raman spectrum of a local corrosion feature is shown in Figure 13. Also in this figure the corrosion feature is divided into three different areas. It can be seen that the intensities of Cu_2O is highest in the outside crystalline oxide area, x', and lowest in the smoother ring-shaped area, y'.[58]

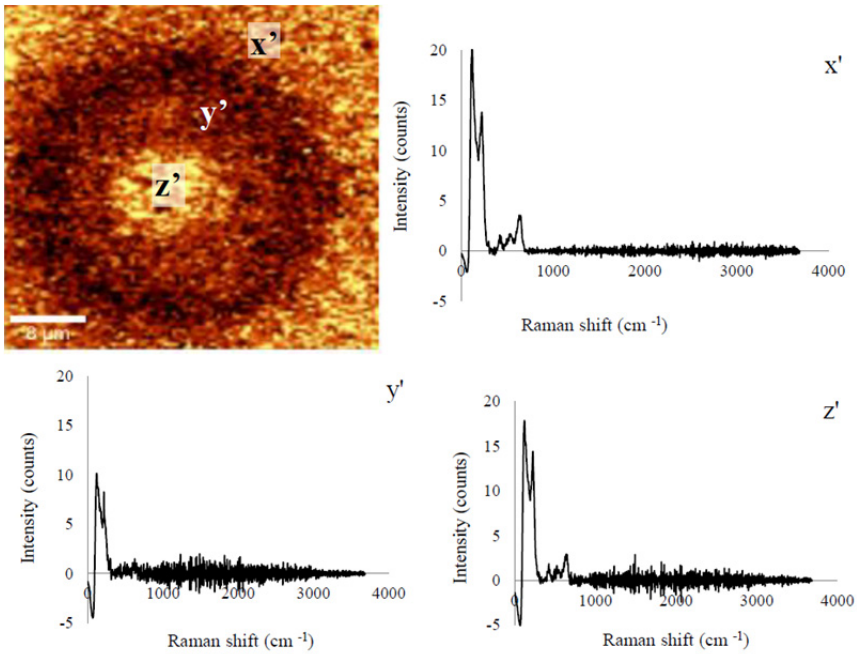

Fig 13. Confocal Raman image and spectra of a local corrosion feature.

The mechanism behind the occurrence of the corrosion features is not fully understood but is presumably of electrochemical nature. Galvanic actions caused by ennoblement of the copper oxide can give rise to anodic and cathodic areas.[59] Slight ennoblement of copper oxide in dilute saline solution has been observed under irradiation by UV-light.[60] A possible formation of electron-hole pairs in the copper oxide can modify the electronic structure of the oxide and create a potential difference between the copper oxide and the copper metal. With water acting as the electrolyte anodic reactions can take place in the metallic copper while the cathodic reactions can take place in the copper oxide.

3.1.2 Pre-oxidized copper cubes in anoxic water

Polished copper cubes were oxidized in air of 90 °C for 24 hours or oxidized in 10 ml of 2.5 mM of H_2O_2 for 36 hours. After the oxidation the copper cubes were irradiated in 10 ml of anoxic pure water for 25-145 hours. The dose rates varied between 0.1 and 0.3 $Gy \cdot s^{-1}$ and the maximum total dose absorbed was 110 kGy.

3.1.2.1 Measured concentration of copper in solution after irradiation of pre-oxidized copper cubes

A series of exposures of copper cubes to different total doses of gamma radiation was performed. The concentration of copper in solution was measured after the exposures and the results are presented in Figure 14 together with previously presented results from Figure 6.

It can be seen in Figure 14 that the concentration of copper in solution is higher when pre-oxidized copper cubes are exposed to total doses from 9-110 kGy in anoxic pure water, than when polished copper cubes are exposed to gamma radiation under similar conditions. Admittedly the data is scattered but the trend is confirmed both for copper cubes pre-oxidized in dry, warm air and in H_2O_2. The yield of copper in solution after irradiations of polished copper cubes is 0.0006±0.0001 $\mu mol \cdot J^{-1}$ while after irradiations of pre-oxidized copper cubes the yield of copper in solution is 0.0011±0.0003 $\mu mol \cdot J^{-1}$. The concentration of copper in solution after reference pre-oxidized copper samples were exposed to 10 ml anoxic pure water for 96 hours was only 0.5 μM. The horizontal line in Figure 14 corresponds to the concentration

of copper in solution measured after oxidation of copper cubes in 25 μmoles of H_2O_2 for 36 hours, approximately 4 μM.

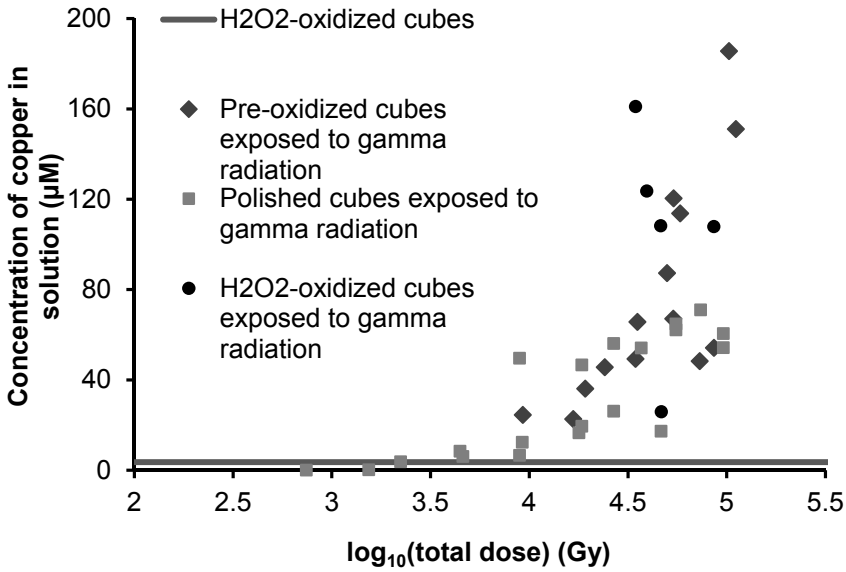

Fig 14. Measured concentrations of copper in solution after irradiations of polished and pre-oxidized copper cubes.

3.1.2.2. Oxide formation during irradiation of pre-oxidized copper cubes

Already by visual inspection it can be seen that the irradiated pre-oxidized copper cubes are more corroded than the reference pre-oxidized copper cubes.

The oxide formed on pre-oxidized copper cubes during gamma irradiation was studied using IRAS. In Figure 15 an IRAS spectrum from a pre-oxidized copper surface irradiated at a dose rate of 0.25 $Gy \cdot s^{-1}$ for 96 hours is shown. The peak at ~650 cm^{-1} corresponds to

Cu_2O.[55] No other peaks were observed in the scanning range between 2000 and 4000 cm^{-1}.

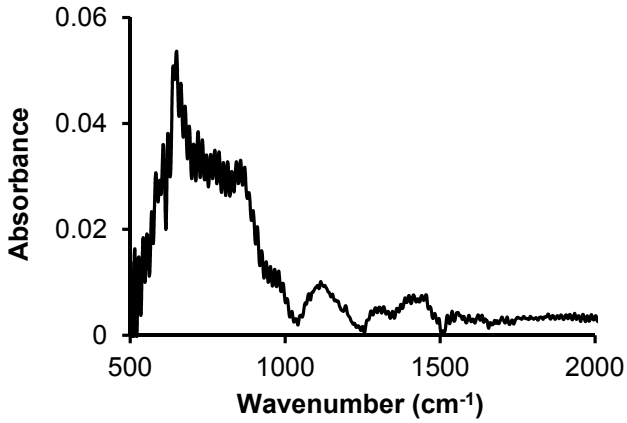

Fig 15. IRAS spectrum of a pre-oxidized copper cube (90°C dry air for 24 hours) exposed to gamma radiation using a dose rate of 0.25 $Gy \cdot s^{-1}$ for 96 hours.

The amount of oxidized copper on the irradiated pre-oxidized copper cubes was measured using cathodic reduction. The expected corrosion products, CuO and Cu_2O, have reduction potentials in the ranges of -0.60 to near -0.80 V (vs. SCE) and from -0.85 to -0.95 V (vs. SCE), respectively.[61] The results from the measurements can be seen in Figure 16. There is almost no difference between the two reference samples exposed to 90 °C air for 24 hours and exposed to 90 °C in air for 24 hours followed by exposure to anoxic water for 145 hours. Judging by the potentials in Figure 16, the main corrosion product formed on the pre-oxidized copper surfaces, both before and after exposure to gamma

radiation, is Cu_2O. This is in agreement with the results from IRAS measurements in Figure 15.

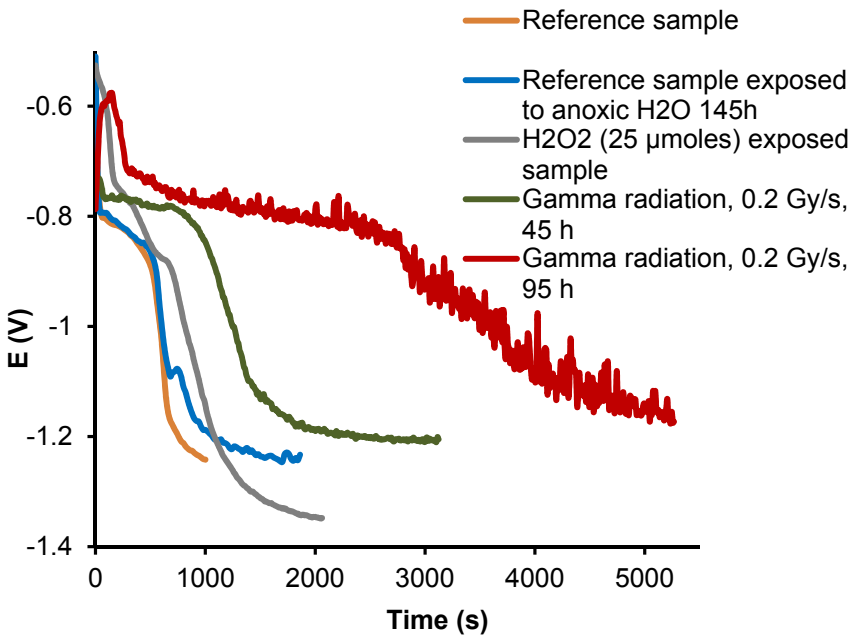

Fig 16. Results from cathodic reduction measurements of irradiated pre-oxidized copper surfaces and reference pre-oxidized copper surfaces.

The amounts of electrons required to reduce the oxidized copper back to metallic copper, for the different exposures in Figure 16, are given in Table 4. On the copper cube exposed to 25 µmoles of H_2O_2 the oxide layer seems to contain both Cu_2O and CuO. From the results presented in Table 4, it can be concluded that only 18 % of the H_2O_2 contributes to oxide formation. The remaining 82 % were consumed via catalytic decomposition and solution reactions.[62]

Table 4. 1) Pre-oxidized in 90 °C air 24 h; 2) Pre-oxidized in 90 °C air 24 h + anoxic water 145 h; 3) H_2O_2 exposed sample (25 µmol); 4) Pre-oxidized in 90 °C air 24 h + gamma radiation 0.2 $Gy \cdot s^{-1}$ in anoxic water 45 h; 5) Pre-oxidized in 90 °C air 24 h + gamma radiation 0.2 $Gy \cdot s^{-1}$ in anoxic water 95 h. The differences between the reference sample and other samples are given within parentheses (no comparison is given for H_2O_2-oxidation).

Experimental conditions	1)	2)	3)	4)	5)
Amount of e^- required to reduce $Cu_{(ox)}$ back to Cu^0 ($\mu mol \cdot cm^{-2}$)	0.39 (0)	0.61 (0.22)	0.74	0.88 (0.49)	2.6 (2.21)

Interestingly, the amount of oxide formed on pre-oxidized copper cubes during irradiation is larger than the amount of oxide formed on polished copper cubes under similar conditions, see also Table 5. The major part of the oxidized copper, after irradiation at a dose rate of 0.2 $Gy \cdot s^{-1}$ for 95 hours, is situated in the oxide layer while less than 0.1 % is released into solution.

3.1.2.3 Formation of local corrosion features during irradiation of pre-oxidized copper cubes

A SEM image from examinations of a reference pre-oxized copper surface, exposed to 90 °C in air for 24 hours, is shown in Figure 17 a. In the SEM image a quite homogeneous oxide layer can be seen. Markings from polishing and small particles are visible on the surface.

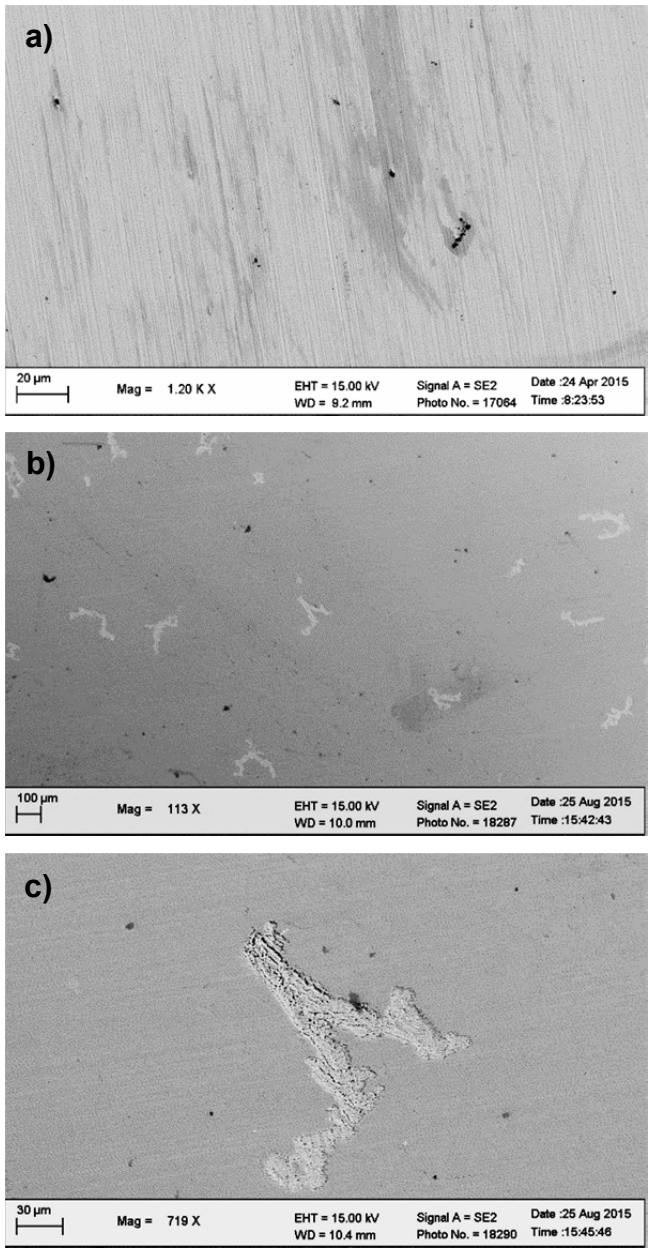

Fig 17 a, b and c. SEM-images of a reference pre-oxidized copper (a) and irradiated pre-oxidized copper (b and c).

SEM images of an irradiated pre-oxidized copper cube reveal widely spread local corrosion features embedded in the oxide layer, see Figure 17 b) and c). Irradiation was performed at 0.25 Gy·s-1 in 10 ml of pure anoxic water for 96 hours.

3.1.3 Impact of homogeneous water radiolysis on the corrosion of copper

To evaluate the impact of radiolysis products formed when gamma radiation is absorbed by anoxic pure water, numerical simulations were performed using MAKSIMA software. When using the reaction scheme given in Table 2, the concentrations of radiolytic species as a function of irradiation time in homogenous aqueous solution can be fairly accurately predicted. The surface area of a copper cube is only 6 cm^2 and therefore the solid surface-area-to-solution-volume-ratio is sufficiently low for surface reactions not to influence the bulk reactions.[22]

The concentrations of H_2O_2 and $HO^{\cdot}$, obtained at a given time for a given dose rate from numerical simulations, are used in Equation 2 and the amount of oxidized copper is obtained by integrating Equation 2 over the reaction time. Since the rate constants for interfacial oxidation of a copper cube is not known the diffusion controlled rate constant is used (10^{-6} $m \cdot s^{-1}$).[16] This will provide the maximum possible amount of oxidized copper and is most probably an overestimation. The results from numerical simulations together with experimental results are given in Table 5.[54]

Table 5. 1) Numerical simulations, irradiation time: 96 h; 2) Experimental value polished cubes: irradiation time: 96 h; 3) Experimental value pre-oxidized cubes, irradiation time: 95 h. The dose rate used in all experiments is 0.2 $Gy \cdot s^{-1}$.

Experimental conditions	1)	2)	3)
Amount of e^- required to reduce $Cu_{(ox)}$ back to Cu^0 ($\mu mol \cdot cm^{-1}$)	0.0014	0.52	2.21

As can be seen in Table 5, the experimental values of oxidized copper vastly exceed the theoretical values. The difference between theory and experimental values for polished copper cubes is more than 350 times and for pre-oxidized copper cubes the difference is even larger, more than 1500 times.

However, it should be noted that the surface area used when performing the calculations using Equation 2, is the geometrical surface area of a copper cube, 6 cm^2. For a polished copper cube this value is probably quite close to the actual surface area. Once the oxidation of the copper surface proceeds during irradiation, an oxide layer is formed and the surface area will increase.

When oxidizing the copper cube using H_2O_2 there is no observation of enhanced corrosion. Instead the oxidized copper corresponds to only a fraction of the consumed oxidant. The only other radiolysis product that can be responsible for the corrosion then is the $HO\cdot$. One speculation could be that the $HO\cdot$, which is a very strong oxidant, is able to oxidize the copper metal through the oxide. If the thermodynamic driving force would be large enough then

electrons could be conducted through the oxide to the oxidant. Due to its very high reactivity, only $HO^{\cdot}$ produced on or very near the copper surface, will be able to react with the surface. Hence, the surface area of the oxide would have strong influence on the rate of the oxidation.

Preliminary data show that when exposing metallic copper powder to different oxidants the yield of oxidized copper increases with increasing oxidizing power of the oxidants used. Results from another preliminary study which also support the theory presented above, is that when copper cubes are irradiated in saline solution, much less corrosion is observed compared to irradiations in pure water. The reason for this can be that the $HO^{\cdot}$ will be scavenged rapidly by Cl^- and HCO_3^- to form other, less oxidative, radical species.

Studies of metal oxide-liquid systems have confirmed an increase in the radiation chemical yield of hydrogen ($G(H_2)$).[17-21] The exact mechanism for this enhanced production is still unknown but it is most probably due to energy transfer from the solid phase into the liquid phase. The effect depends on the type of oxide, the surface morphology and the solid surface-area-to-solution-volume-ratio. The $G(H_2)$ increases with decreasing water film thickness. Some studies have also confirmed increased radiation chemical yields of hydroxyl radicals ($G(HO^{\cdot})$) and hydrogen peroxide ($G(H_2O_2)$) in these type of systems.[63-65] Nanoporous stainless steel, nickel based alloy or gold were impregnated with a $HO^{\cdot}$ scavenger. During irradiation of systems containing water and the nanoporous materials, the $HO^{\cdot}$ formation at the solid surfaces was 2-6 times

higher compared to the formation of HO· in pure bulk water. The increase of the HO· production during irradiation can be used to explain the detected increase of H_2O_2 production under similar conditions. If the HO· is not scavenged it can recombine to form H_2O_2. The increase of H_2O_2 formation is greater under low dose rate irradiations and at high solid surface-area-to-solution-volume-ratios.

It is interesting to note that neither CuO nor Cu_2O belong to the group of metal oxides which enhance the production of H_2.[19, 66] If the radiation chemical yield of HO· would be higher than expected on the surface, than this would in turn reduce the yield of H_2.

To conclude, a dramatic increase in specific surface area together with a higher radiation chemical yield of HO· could be major phenomena when explaining the observed radiation enhanced corrosion process.

3.1.4 Polished copper cubes in humid argon

Polished copper cubes were irradiated for 96 hours at a dose rate of 0.13 $Gy \cdot s^{-1}$ in water-saturated argon (100 % RH) at ambient temperature.

3.1.4.1 Oxide formation during irradiation of polished copper cubes in humid argon

After irradiations the exposed copper surfaces were examined using IRAS. In Figure 18 an IRAS spectrum is shown. There is a characteristic Cu_2O peak at wavenumber ~650 cm^{-1} and this is the only peak observed within the scanning range (500-4000 cm^{-1}).

The very strong peak indicates a quite thick Cu_2O layer present on the copper surface.

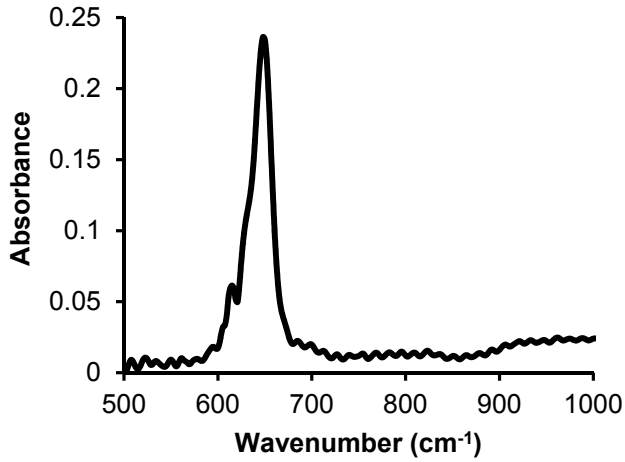

Fig 18. IRAS spectrum of a sample exposed to gamma radiation in water-saturated Argon at a dose rate of 0.13 $Gy \cdot s^{-1}$ for 96 hours.

Reference experiments were also performed where copper cubes were irradiated in dry argon at a dose rate of 0.13 $Gy \cdot s^{-1}$ and, as expected, no corrosion products were detected.

The oxide formation during irradiations in water-saturated argon was also studied using cathodic reduction. It can be seen clearly in Figure 19 that the amount of oxidized copper is many times higher on the irradiated copper surface than on the unirradiated reference copper surface. Also, judging by the potential range, the oxide layer contains a small amount of CuO but the main part is Cu_2O.

The amount of electrons required to reduce all the oxidized copper back to metallic copper is given in Table 6.

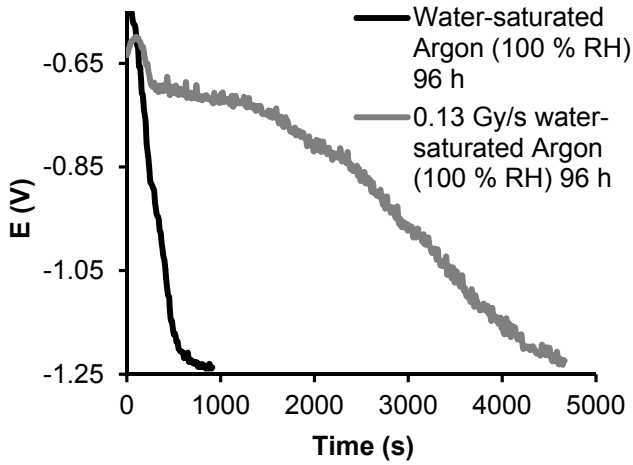

Fig 19. Results from cathodic reduction measurements of polished copper surfaces, irradiated and unirradiated, in water-saturated Argon.

3.1.4.2 Formation of local corrosion features during irradiation of polished copper cubes in humid argon

Surface characterizations using SEM reveal local corrosion features on copper surfaces irradiated in water-saturated argon. The corrosion features are spread all over the surface and are of different sizes and shapes. The SEM images can be seen in Figure 20 a) and b).

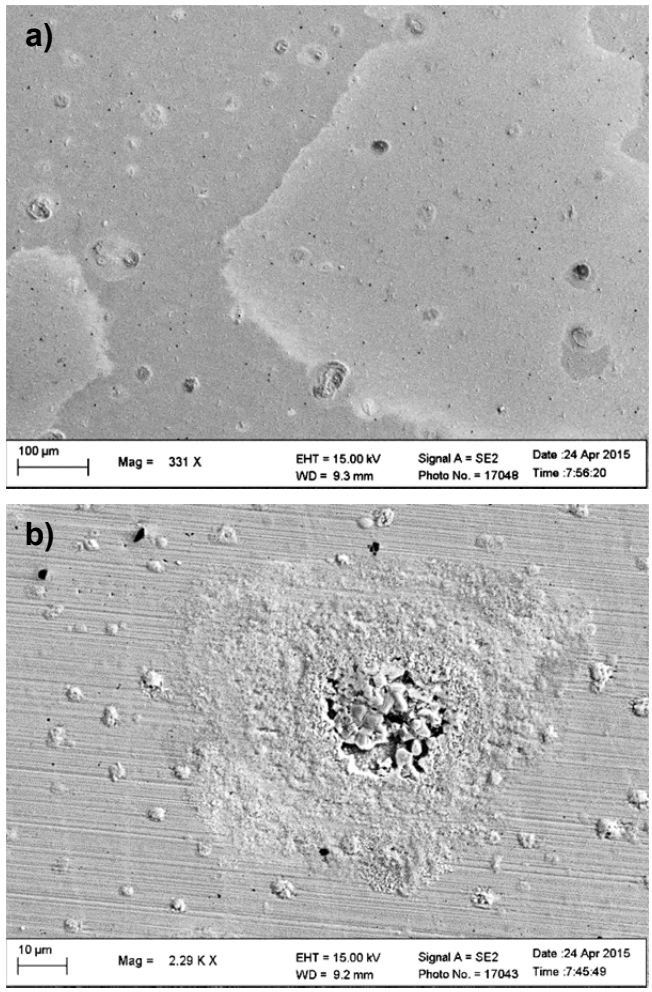

Fig 20 a) and b). SEM images of a polished copper surface irradiated in water-saturated argon at a dose rate of 0.13 $Gy \cdot s^{-1}$ for 96 hours.

3.1.5 Humid air

Copper cubes were irradiated at dose rates of 0.1-0.3 $Gy \cdot s^{-1}$ for 96 hours in air of 60 % or 100 % RH. The water films on copper in air of 60 % and 90 % RH consist of approximately 8 and 18

monolayers respectively. At 100 % RH the number of monolayers is not meaningful to measure as they increase continuously due to condensation of the moisture.[8, 9]

3.1.5.1 Oxide formation during irradiation of polished copper cubes in humid air

Surface examination of a copper cube exposed to water-saturated air, using IRAS, can be seen in Figure 21.

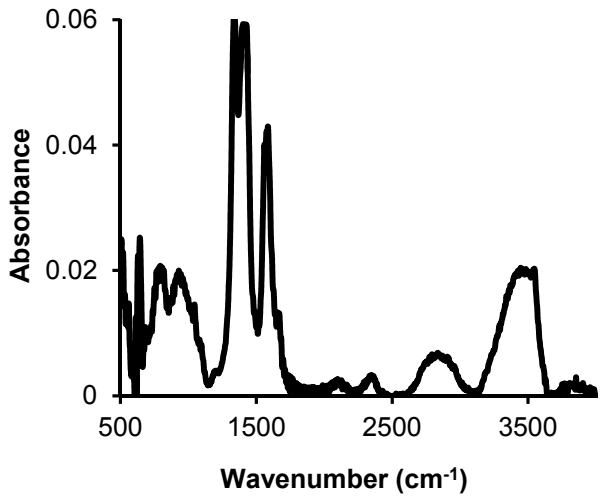

Fig 21. IRAS spectrum of a copper surface irradiated at a dose rate of 0.13 $Gy \cdot s^{-1}$ in air of 100 % RH for 96 hours.

Several different peaks can be seen in the IRAS spectrum from a copper surface irradiated in water-saturated air compared to the IRAS spectrum of a copper surface exposed to water-saturated argon. The peak at wavenumbers ~650 cm^{-1} corresponds to Cu_2O[55] while the peaks at wavenumbers ~1320-1440cm^{-1}, ~3555 cm^{-1} and

~1590 cm^{-1} correspond to copper nitrates, $Cu_4(NO_3)_2(OH)_6$ and $Cu(NO_3)_2$ respectively.[67, 68] CuO has a wide peak close to the cutoff frequency at wavenumbers ~520-560 cm^{-1} and as can be seen in Figure 21 the presence of CuO cannot be ruled out.[56]

In Figure 22 an IRAS spectrum of a copper surface exposed to gamma radiation at a dose rate of 0.14 $Gy \cdot s^{-1}$ for 96 hours in air of 60 % RH, can be seen. This spectrum is quite similar to the spectrum in Figure 21, with the exception of the peak corresponding to Cu_2O. There is no indication of the presence of Cu_2O on the copper surface. Also the peak at wavenumbers ~1590 cm^{-1} corresponding to $Cu(NO_3)_2$ is smaller and wider than in the previous spectrum. The sharp peak at wavenumber ~1050 cm^{-1} may correspond to a copper carbonate, $Cu2(OH)_2(CO_3)$.[69]

An IRAS spectrum of a copper surface exposed to gamma irradiation in air of 60 % RH at a dose rate of 0.14 $Gy \cdot s^{-1}$ for 96 hours followed by immersion in anoxic pure water under gamma irradiation at a dose rate of 0.2 $Gy \cdot s^{-1}$ for 96 hours, is shown in Figure 23.

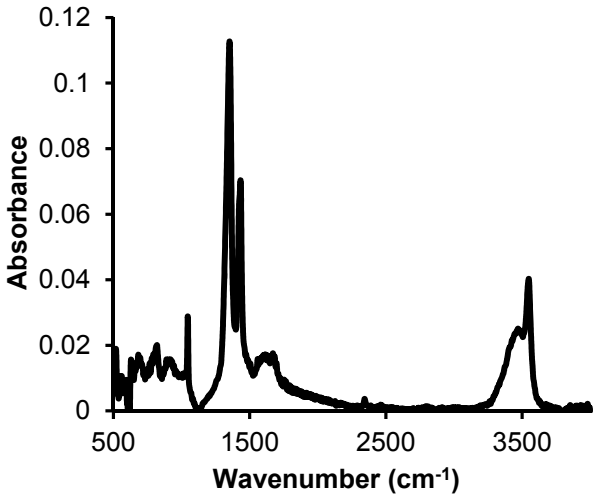

Fig 22. IRAS spectrum of a sample exposed to gamma radiation in air of 60 % RH at a dose rate of 0.14 $Gy \cdot s^{-1}$ for 96 hours.

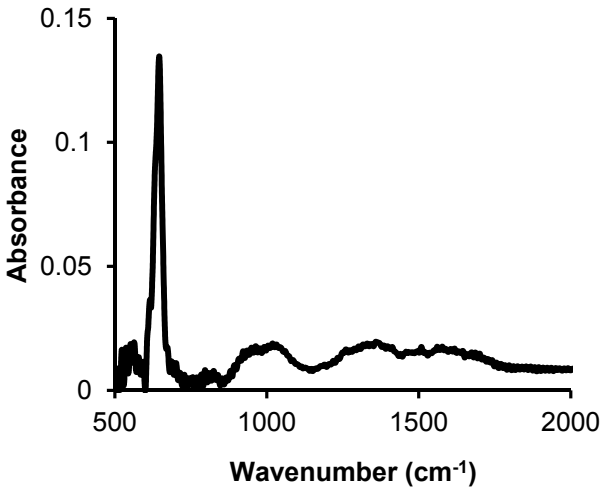

Fig 23. IRAS spectrum of a copper surface irradiated at a dose rate of 0.14 $Gy \cdot s^{-1}$ in air of 60 % RH for 96 hours followed by exposure to anoxic water under gamma radiation at a dose rate of 0.2 $Gy \cdot s^{-1}$ for 96 hours.

The strong peak at wavenumbers ~650 cm^{-1} corresponds to Cu_2O[55] and the high intensity indicates a thick copper oxide layer present at the surface. No signs of copper nitrates are detected and the reason for this is probably the high solubility of copper nitrates in water.[70] The formation of Cu_2O during gamma irradiation in anoxic pure water is in agreement with earlier presented results. The phenomenon of the formation of copper nitrates during irradiation followed by dissolution during water exposure might be something to take into consideration in the handling of copper canisters for spent nuclear fuel. Copper nitrates can be formed on the canister surface when the canister is exposed to air. If the canister is later exposed to water the copper nitrates can be washed off and a loss of material can occur.

Results from cathodic reduction measurements from copper surfaces exposed to air of 60 % RH, air of 60 % RH followed by immersion in anoxic water, irradiated in air of 60 % RH, irradiated in air of 60 % RH followed by immersion in anoxic water and irradiated in air of 60 % RH followed by irradiation in anoxic water can be seen in Figure 24.

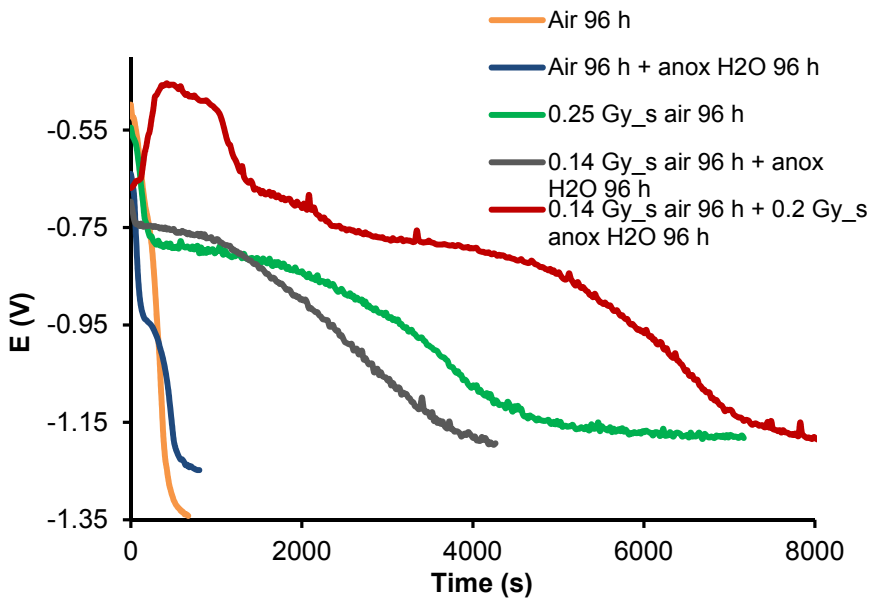

Fig 24. Results from cathodic reduction measurements of polished copper surfaces, irradiated and unirradiated, in humid air.

On both reference copper samples, exposed to air of 60 % RH for 96 hours and exposed to air followed by immersion in pure anoxic water for 96 hours, the corrosion layers are quite thin. A significantly thicker corrosion layer is formed on the copper cube exposed to gamma irradiation in air of 60 % RH at a dose rate of 0.25 $Gy \cdot s^{-1}$ for 96 hours. This is most probably due to the formation of nitric acid originating from the gamma radiolysis of humid air.[14] The thickness of the corrosion layer formed on copper cubes exposed to gamma irradiation in air of 60 % RH followed by immersion in anoxic pure water is similar as on copper cube irradiated in air of 60 % RH. When exposing copper cubes to gamma irradiation in air of 60 % RH at a dose rate of 0.14 $Gy \cdot s^{-1}$

for 96 hours followed by irradiation in anoxic pure water at a dose rate of 0.2 $Gy \cdot s^{-1}$ for 96 hours, the corrosion layer is even thicker than on all previous samples. A summary of the results from cathodic reductions is given in Table 6.

Table 6. 1) Air 60 % RH 96 h; 2) Irradiation in air 60 % RH 96 h 0.25 $Gy \cdot s^{-1}$; 3) Air 60 % RH 96 h + anoxic H_2O 96 h; 4) Irradiation in air 60 % RH 0.14 $Gy \cdot s^{-1}$ 96 h + anoxic H_2O 96 h; 5) Irradiation in air 60 % RH 0.14 $Gy \cdot s^{-1}$ 96 h + irradiation in anoxic H_2O 0.2 $Gy \cdot s^{-1}$ 96 h; 6) Water-saturated argon 96 h; 7) Irradiation in water-saturated argon 96 h 0.13 $Gy \cdot s^{-1}$; 8) Water-saturated air 96 h; 9) Irradiation in water-saturated air 96 h 0.13 $Gy \cdot s^{-1}$;

Experimental conditions	1)	2)	3)	4)	5)	6)	7)	8)	9)
Amount of e^- required to reduce $Cu_{(ox)}$ to Cu^0 ($\mu mol \cdot cm^{-2}$)	0.25	2.3	0.27	2.1	3.8	0.29	2.3	0.4	2.9

The radiation induced corrosion of copper is more efficient in humid atmosphere than in bulk water. The amount of oxidized copper after irradiation in water-saturated argon is several times higher than after irradiation in anoxic water. This can be explained to some extent if considering the $HO\cdot$ to be the main oxidant, as proposed in previous section. Due to the high reactivity of the $HO\cdot$ it can only diffuse a very short distance before it is consumed and therefore it will never take part in surface reactions if produced in bulk water. By less shielding due to the absence of bulk water more energy can be absorbed by the thin water film on the copper

surface. Also fewer amounts of stable molecular radiolysis products, such as H_2O_2, will accumulate in a thin water film than in bulk water e.g. less scavenging of $HO\cdot$ by H_2O_2 will occur. Another reason why H_2O_2 might decrease the rate of oxidation of copper is that H_2O_2 can occupy sites on the surface during catalytic decomposition preventing $HO\cdot$ to reach the surface. Only a small contribution to the oxidation of copper comes from H_2O_2, most of it is consumed by catalytic decomposition or solution reactions.[62] This might explain the increased efficiency of radiation induced corrosion of copper in water-saturated argon compared to radiation induced corrosion of copper in anoxic pure water. The rate of corrosion will probably increase with increasing water film thickness up to a certain point corresponding to a very thin water film. Beyond this point the $HO\cdot$ produced in the water film will no longer be able to reach the copper surface.

In Figure 25 SEM images of two copper surfaces can be seen. Copper cubes were exposed to gamma irradiation at a dose rate of 0.25 $Gy\cdot s^{-1}$ for 96 hours in air and to gamma irradiation at a dose rate of 0.16 $Gy\cdot s^{-1}$ for 96 hours followed by immersion in anoxic pure water for 96 hours.

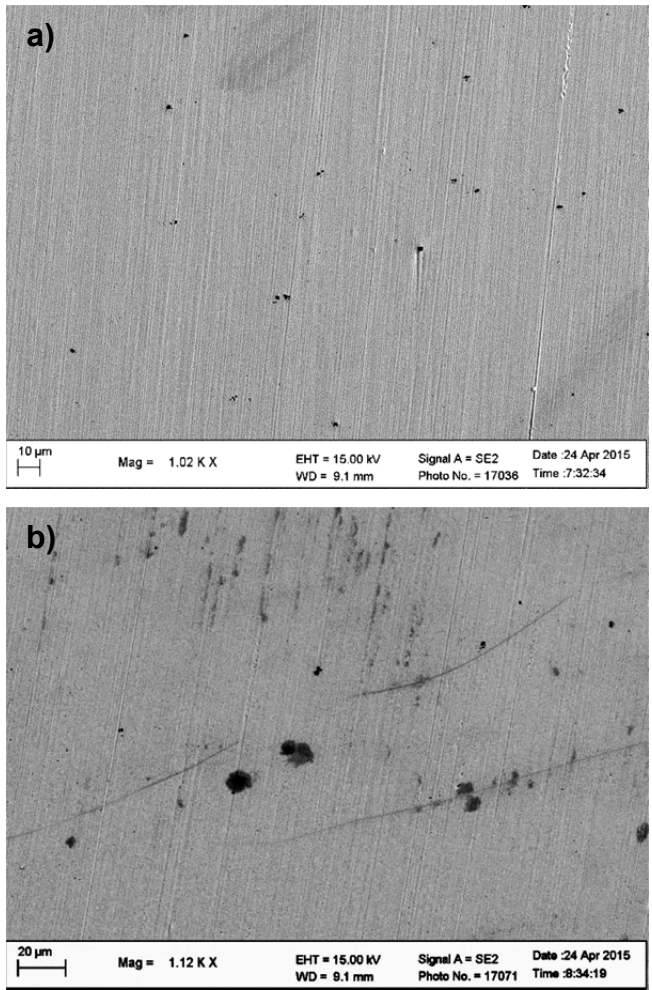

Fig 25 a) and b). SEM images of a) a copper surface irradiated at a dose rate of 0.25 $Gy \cdot s^{-1}$ for 96 hours in air and b) a copper surface irradiated in air at followed by exposure to anoxic water.

When comparing the two images it can be noted that the copper surface in image a) looks quite homogeneous whiles the copper surface in image b) looks more heterogeneous. In both SEM

images small pits and particles can be seen together with markings from polishing. The more heterogeneous appearance of the copper surface in Figure 25 b) might be caused by dissolution of copper nitrates, formed under irradiation in humid air, during the exposure to water.

As a complement to the SEM images AFM surface profiles were used to confirm the presence of pits and particles on the copper surface. Figure 26 shows an AFM surface profile following one of the lines from polishing over an area with what appears to be pits in the surface. The profile shows small pits of approximately 0.05–0.1 μm depth.

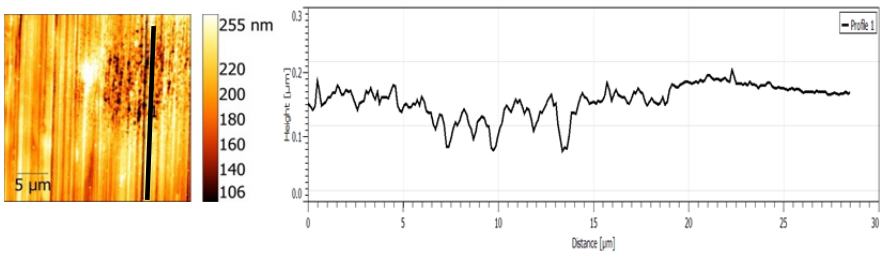

Fig 26. AFM image and surface profile of small pits in a copper surface irradiated at a dose rate of 0.11 $Gy \cdot s^{-1}$ for 96 hours in air of 60 % RH.

In Figure 27 surface profiles crossing over two particles on the copper surface are shown. The heights of the particles are approximately 0.5-0.7 μm.

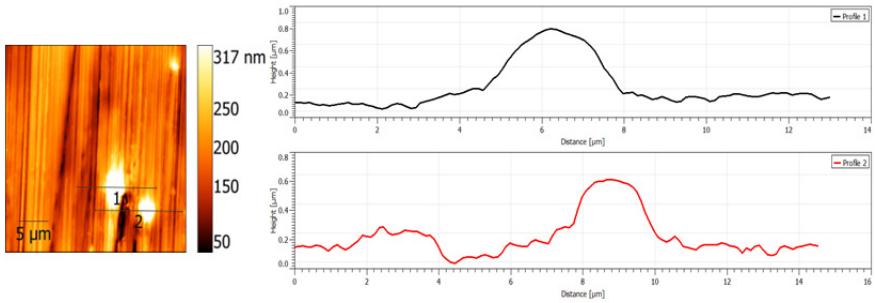

Fig 27. AFM image and surface profiles of particles on a copper surface irradiated at a dose rate of 0.11 $Gy \cdot s^{-1}$ for 96 hours in air of 60 % RH

The concentration of copper in solution was measured using ICP-OES and the results are presented in Figure 28.

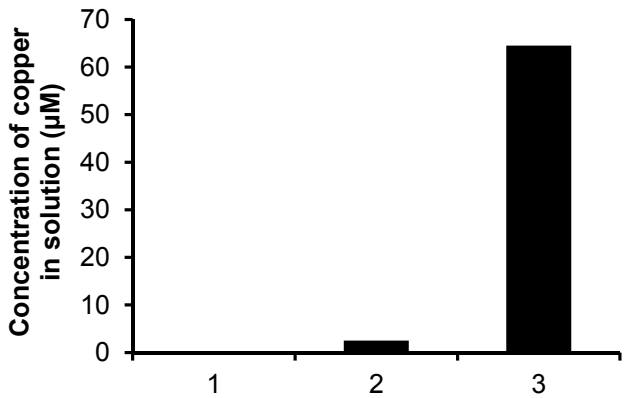

Fig 28. Concentration of copper in solution. 1) Oxidation in air for 96 hours followed by exposure to anoxic pure H_2O for 96 hours; 2) γ-irradiation in air for 96 hours, 0.1 $Gy \cdot s^{-1}$, followed by exposure to anoxic pure H_2O for 96 hours; 3) γ-irradiation in air for 96 hours, 0.14 $Gy \cdot s^{-1}$, followed by exposure to γ-irradiation in anoxic pure H_2O for 96 hours, 0.2 $Gy \cdot s^{-1}$.

When a copper cube was first irradiated at a dose rate of 0.14 $Gy \cdot s^{-1}$ for 96 hours in air of 60 % RH followed by irradiation at a dose rate of 0.2 $Gy \cdot s^{-1}$ for 96 hours in 10 ml of anoxic pure water, the concentration of copper in solution was approximately 65 µM (solution 3 in Figure 28). The concentration of copper in unirradiated solutions (solution 1 and 2 in Figure 28) was only 0.5-5 µM. The concentration of copper in solution 2 might originate from dissolved copper nitrates.

3.2 Kinetics and mechanisms between H_2O_2 and copper and copper oxides

To further understand the interfacial processes between copper and the stable radiolysis product, H_2O_2, the consumption of H_2O_2 in the presence of metallic copper and copper oxides were studied. Also the formation of formaldehyde (CH_2O) from the reaction between methanol (CH_3OH) and $HO\cdot$ was studied. The concentration of copper in solution was measured using ICP-OES after the consumption of H_2O_2 was complete. From XPS-measurements presented in a previous section, Cu_2O is expected to be the main corrosion product forming on metallic copper powder during the reaction with H_2O_2.

3.2.1 Kinetics of the reactions between H_2O_2 and copper and copper oxides

The consumption of H_2O_2 on various amounts of metallic copper powder (Cu-powder), Cu_2O-powder and CuO-powder was monitored using spectrophotometry as a function of reaction time.

Initial experimental conditions were 50 ml of 0.5 mM of H_2O_2 of ambient temperature, with continuous N_2 purging. The pH for all solutions was approximately 6 before, during and after the reactions. In Figure 29 – 31, the concentration of H_2O_2 as a function of reaction time is given for reactions with Cu-powder, Cu_2O-powder and CuO-powder.

As can be seen in Figures 29-31 the rate of consumption of H_2O_2 is increasing with increasing amount of powders. To be able to compare the reactivity towards H_2O_2 of the three powders, the second-order rate constants (k_2 ($m \cdot s^{-1}$)) are determined. The slopes, of the first-order rate constants for the reactions between H_2O_2 and the three powders plotted against solid surface-area-to-solution-volume ratios, are calculated to obtain the second-order rate constants.

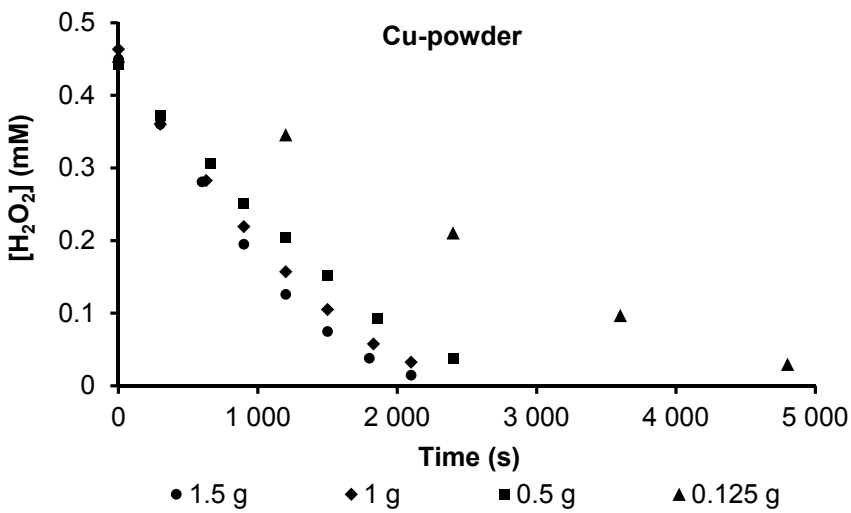

Fig 29. The concentration of H_2O_2 as a function of reaction time on Cu-powder.

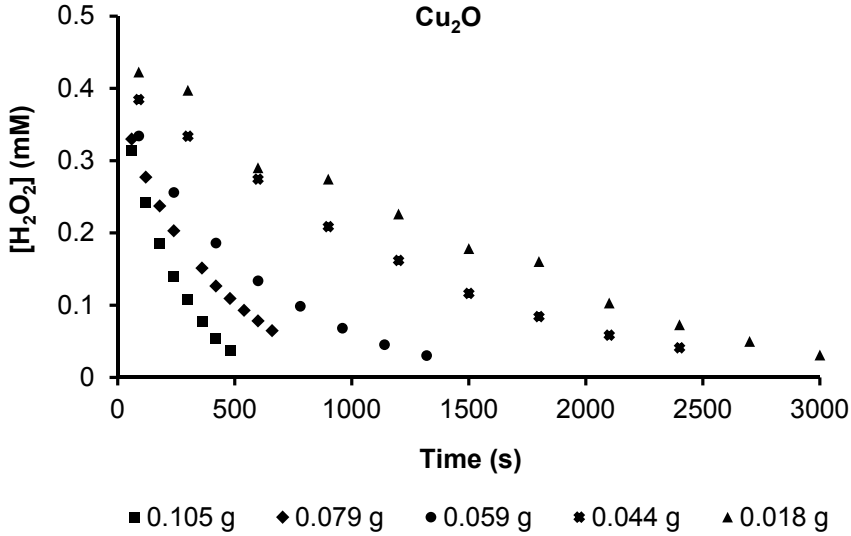

Fig 30. The concentration of H_2O_2 as a function of reaction time on Cu_2O-powder. © The Royal Society of Chemistry 2015

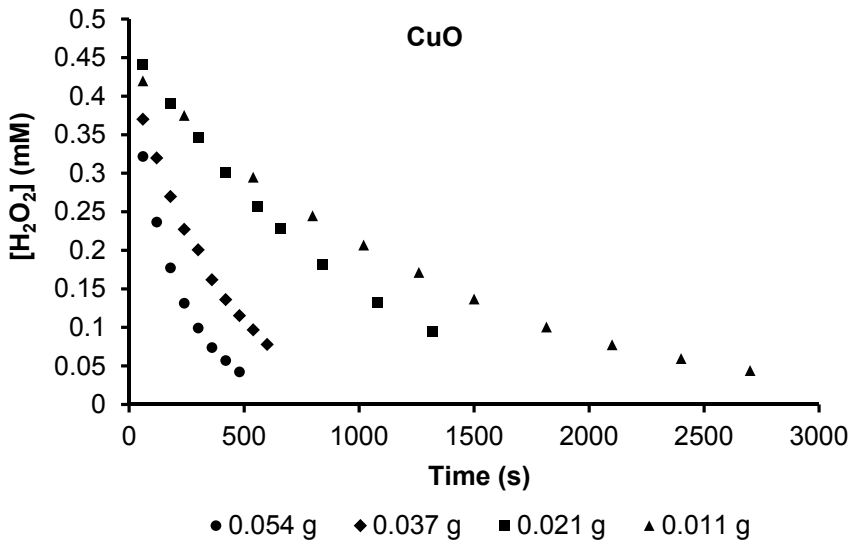

Fig 31. The concentration of H_2O_2 as a function of reaction time on CuO-powder. © The Royal Society of Chemistry 2015

Admittedly, the reaction order of the reactions presented in Figures 29-31 is not always one and to circumvent this problem, only the initial parts of the plots are used for determination of the first-order rate constants.

In Figure 32, the first-order rate constants for the reactions between H_2O_2 and Cu-, Cu_2O- and CuO-powder are plotted against solid surface-area-to-solution-volume ratios. The slopes of the three curves are calculated to obtain the second-order rate constants. Judging from Figure 32, Cu_2O is the powder which displays the highest reactivity towards H_2O_2.

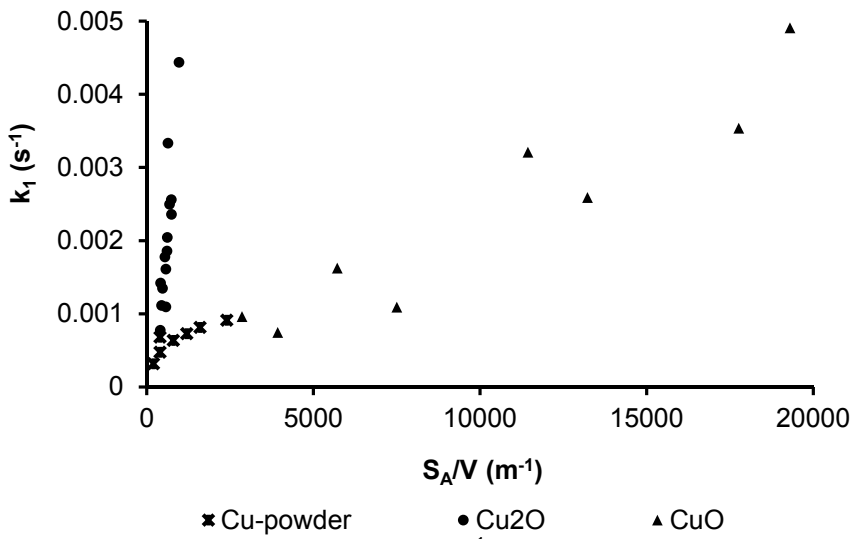

Fig 32. First-order rate constants (k_1 (s^{-1})) as a function of solid surface-area-to-solution-volume ratios.

It must be kept in mind though that the particle sizes for the three powders are very different and therefore the powders have different diffusion limited rate constants. Larger particles have a lower diffusion limited rate constant than smaller particles. The sizes of the particles are estimated from SEM examinations of the three powders. Comparisons of surface reactivity between Cu-, Cu_2O- and CuO-powder are made by comparing the estimated size normalized relative rate constants for the respective powder.[71]

Figure 33 is an enlargement of the first-order rate constants for consumption of H_2O_2 on Cu_2O-powder plotted against solid surface-area-to-solution-volume ratios. There it can be seen that for solid surface-area-to-solution-volume ratios below 400 m^{-1}, the consumption of H_2O_2 is independent of the surface area of the oxide. This behavior can probably be attributed either to H_2O_2 reacting with dissolved Cu(I) in the Fenton reaction or to H_2O_2 reacting with Cu(I) and Cu(II) in the Haber-Weiss reaction. [72-74] The solubility of Cu_2O and CuO at pH 6 is 1 and 10 μM respectively.[75] For solid surface-area-to-solution-volume ratios above 400 m^{-1}, the surface reactions become competitive to the solution reactions and the rate of H_2O_2 consumption is increasing with increasing amount of Cu_2O. The second-order rate constant for H_2O_2 consumption on Cu_2O-powder is obtained from solid surface-area-to-solution-volume ratios above 400 m^{-1}. These solution reactions are not observed in the reactions between H_2O_2 and Cu- and CuO-powder.

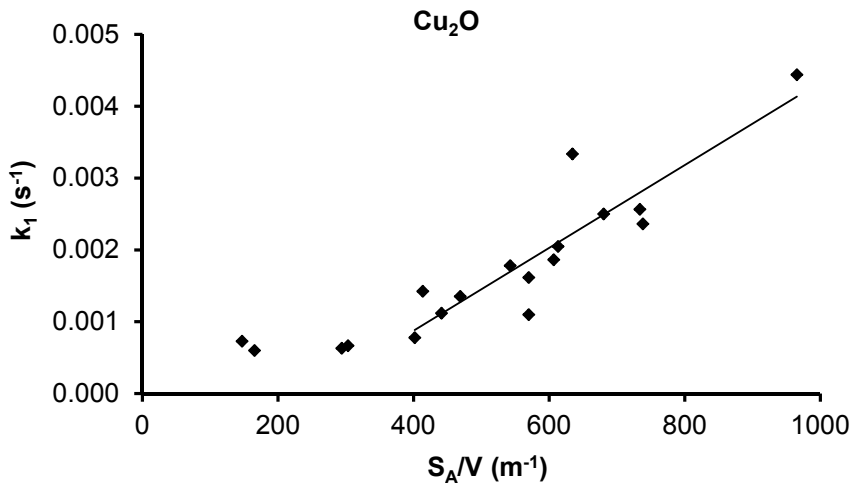

Fig 33. An enlargement of the first-order rate constants k_1 (s^{-1}) for consumption of H_2O_2 on Cu_2O-powder plotted against solid surface-area-to-solution-volume ratios.

The diffusion limited rate constant for a reaction between reactants in a solution and reactants at a particle surface is inversely proportional to the particle size. By multiplying the second-order rate constants, calculated from the slopes of the plots in Figure 32, with each particle size and comparing them with each other, the estimated size normalized relative rate constants are obtained.[71] In Table 7 the constants are given together with powder characteristics. It can be concluded that CuO is less reactive towards H_2O_2 than Cu and Cu_2O. Cu_2O appears to be the most reactive of the three powders. This is most probably due to the fact that H_2O_2 is catalytically decomposed on CuO, while on Cu-powder and Cu_2O, electron-transfer is an additional possibility.

Table 7. 2nd-order rate constants, k_2 ($m \cdot s^{-1}$), and the estimated size normalized relative rate constants (Arb.) for the consumption of H_2O_2 on Cu-, Cu_2O- and CuO-powder. Also B.E.T.-surface areas ($m^2 \cdot g^{-1}$) and estimated particle sizes (µm) are presented. © The Royal Society of Chemistry 2015

Powders	Estimated particle size (µm)	B.E.T.-surface area ($m^2 \cdot g^{-1}$)	2nd-order rate constant, k_2 ($m \cdot s^{-1}$)	Estimated size normalized rate constant (Arb.)
Cu	10-100	0.1	$(2.2 \pm 0.6) \cdot 10^{-7}$	100-1000
Cu_2O	0.5-15	0.5	$(5.8 \pm 0.8) \cdot 10^{-6}$	130-4000
CuO	0.1-10	17.9	$(2.2 \pm 0.3) \cdot 10^{-7}$	1-100

3.2.2 Mechanisms of the reactions between H_2O_2 and copper and copper oxides

CH_3OH was used as a radical scavenger to quantify the impact of catalytic decomposition of H_2O_2 on Cu-, Cu_2O- and CuO-powder. The amount of CH_2O formed in the reaction between $HO\cdot$ and CH_3OH can be determined by spectrophotometry. When H_2O_2 is consumed on the surface of CuO-powder the only pathway for H_2O_2 to react is via catalytic decomposition. The other two powders can also be oxidized by H_2O_2. The yield of CH_2O from CH_3OH and $HO\cdot$ under homogeneous anoxic conditions is only 14 %[34] and therefore the concentrations of CH_2O detected in this work are expected to be quite low. In Figure 34-36 the production of CH_2O and the consumption of H_2O_2 are plotted against reaction time. The solid surface-area-to-solution-volume ratios are the same for all three powders, 4600 ± 200 m^{-1}.

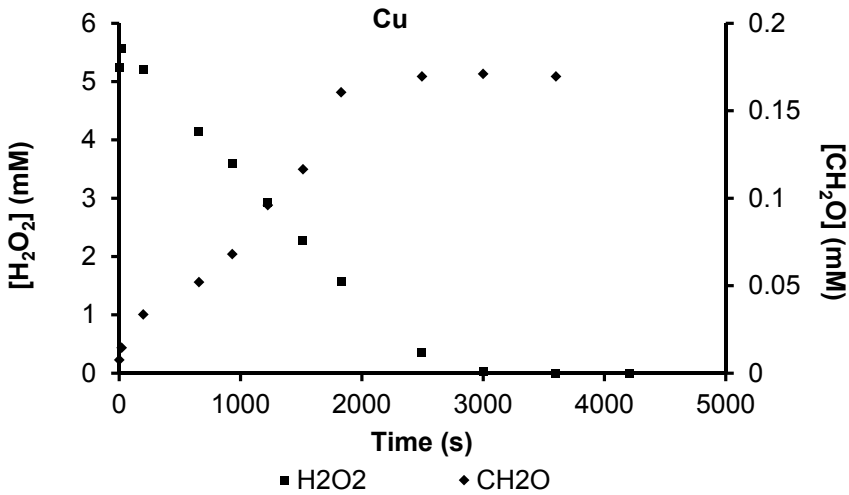

Fig 34. The consumption of H_2O_2 and the production of CH_2O as a function of reaction time for Cu-powder. © The Royal Society of Chemistry 2015

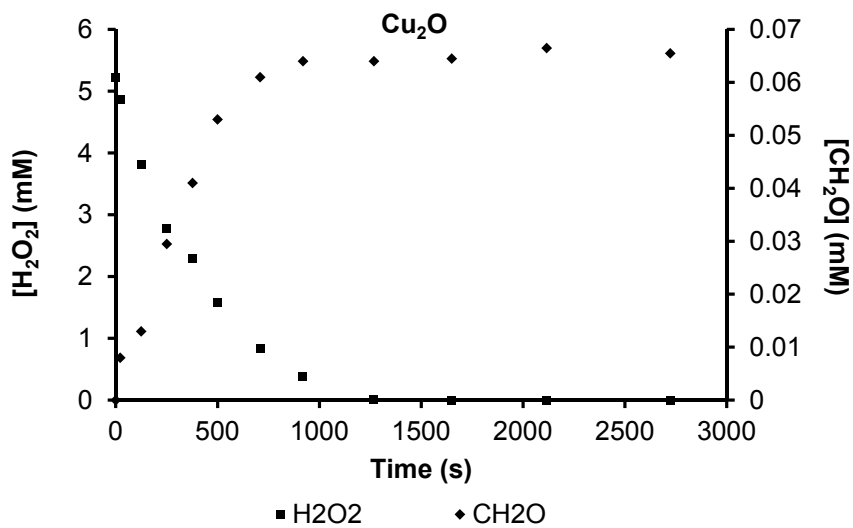

Fig 35. The consumption of H_2O_2 and the production of CH_2O as a function of reaction time for Cu_2O-powder. © The Royal Society of Chemistry 2015

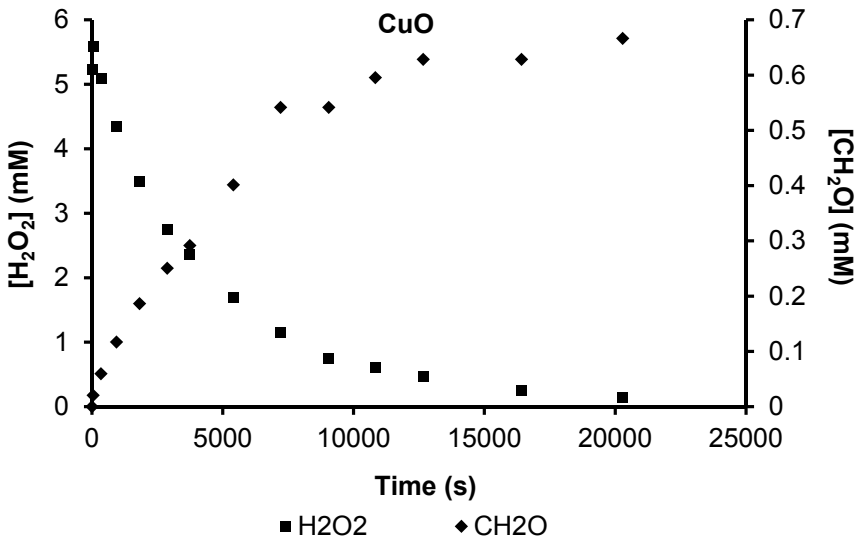

Fig 36. The consumption of H_2O_2 and the production of CH_2O as a function of reaction time for CuO-powder. © The Royal Society of Chemistry 2015

As expected, it can be seen that the yield of CH_2O is clearly highest for CuO because the only pathway for H_2O_2 consumption is trough catalytic decomposition. The lower yield of CH_2O for Cu and Cu_2O is probably due to the competition between surface reactions and solution reactions.

3.2.3 Reactions between H_2O_2 and copper cubes

XPS-measurements show that the main corrosion product formed on a copper cube after exposure to H_2O_2 is Cu_2O with only a small contribution from CuO.[54] Cu_2O will be the oxide closest to the copper metal with CuO on top. In Figure 37 the consumption of

H_2O_2 and the production of CH_2O from the reactions between H_2O_2 and copper cubes are given. The reactions are monitored both for polished copper cubes and pre-oxidized (by 10 ml of 2.5 mM H_2O_2) copper cubes. The solid surface-area-to-solution-volume ratios are «400 m^{-1} in the reactions with copper cubes. Therefore the consumption of H_2O_2 should be governed mainly by solution Fenton- or Haber-Weiss-reactions. Hence, the results given in Figure 37 can only be attributed to surface reactivity to a small extent.

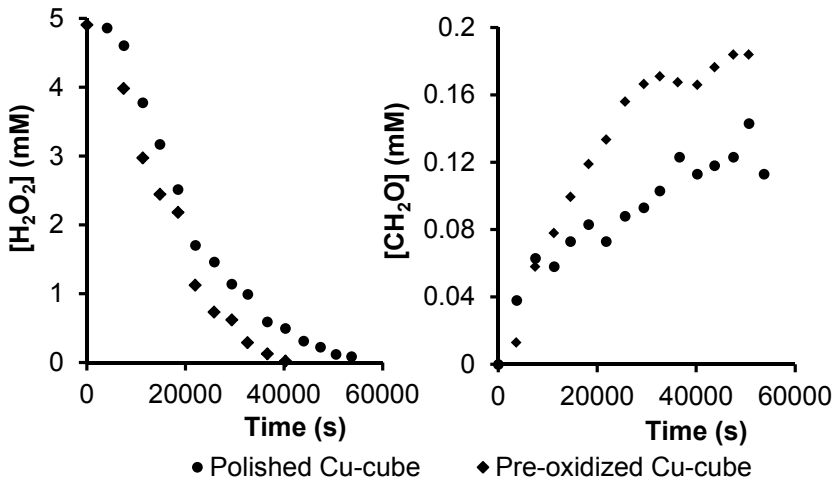

Fig 37. The consumption of H_2O_2 and the production of CH_2O as a function of reaction time for copper cubes. © The Royal Society of Chemistry 2015

It can be seen that the consumption of H_2O_2 on the pre-oxidized copper cube is slightly faster than on the polished copper cube. This is probably due to a larger surface area and immediate

dissolution of copper ions from the already present oxide layer. Also the yield of CH_2O is higher for the pre-oxidized copper cube and this too can probably be attributed to the presence of the oxide layer from the very beginning.

As already mentioned in a previous section, when measuring the concentration of copper in solution after 50 ml of 0.5 mM of H_2O_2 was consumed on a polished copper cube, it is not at all in agreement with the concentrations of copper in solution after copper cubes were exposed to gamma irradiation in anoxic pure water. Consequently, the H_2O_2 produced in gamma radiolysis cannot be the responsible oxidant for the radiation enhanced corrosion of copper. In the mechanistic study when using CH_3OH as a radical scavenger it is proved that $HO^{\cdot}$ species are formed in the unirradiated system with H_2O_2 and copper. Hence, this system should provide an environment similar as the one occurring during irradiations of copper in anoxic water. Still, it is obvious that the surface bound $HO^{\cdot}$ species formed from catalytic decomposition of H_2O_2 do not influence the release of copper into solution as observed in irradiated systems.

3.3 Direct impact of radiation induced corrosion of copper on the integrity of copper canisters for spent nuclear fuel storage

Oxidation of copper in aqueous environment during exposure to total gamma doses, equivalent to the total doses expected to be absorbed by an outer canister surface during the initial hundred years in a deep repository, will not directly threaten the integrity of

the canister. Average oxide layer thicknesses between 0.5 and 1 μm were obtained after irradiations of copper in humid air, humid argon and anoxic water. Also local corrosion features with pit depths of 0.8-0.9 μm were detected after irradiations in anoxic water.

A dose rate dependence was discovered where a lower dose rate during longer irradiation times, gives a higher yield of copper in solution, compared to a higher dose rate and shorter irradiation time, ending up at the same total dose. The dose rates expected on an outer copper canister surface in a repository for spent nuclear fuel are 10 000 times lower and the radiation exposure times will be 10 000 times longer, compared to the conditions in this work.

Interactions between the process of radiation induced corrosion of copper and other copper corrosion processes, such as corrosion by sulfur, atmospheric corrosion, stress corrosion or microbial corrosion, are not taken into consideration in this work.

4. Conclusions

- Gamma irradiated copper samples are always significantly more corroded than corresponding reference samples.
- Exposure of polished copper samples to gamma radiation in anoxic pure water enhances the corrosion process by several hundred times compared to what is expected from the formation of oxidative radiolysis products.
- No enhanced corrosion of copper is observed when exposing copper samples to hydrogen peroxide. The hydroxyl radical species formed on copper oxide surfaces from decomposition of hydrogen peroxide does not influence the release of copper into solution.
- If the polished copper sample is covered by a thin water film the radiation induced corrosion process is more efficient than if the polished copper sample is submerged in water.
- The main corrosion product formed during gamma irradiation of copper in anoxic pure water is Cu_2O together with a small amount of CuO. During exposure of copper to gamma radiation in humid air also copper nitrates are formed.
- Exposure of pre-oxidized copper samples to gamma radiation in anoxic pure water enhances the corrosion process further. Both the oxide growth and the release of copper into solution are greater on pre-oxidized copper samples compared to polished copper samples.

- The main part of the oxidized copper is present as an oxide layer on the copper surface and a minor part is released into the aqueous environment.
- Both the concentration of copper in solution and amount of oxidized copper after exposure of copper to gamma radiation is increasing with increasing absorbed total dose. There is a dose rate dependence for the release of copper into solution where a lower dose rate during a longer irradiation time gives a slightly higher amount of copper in solution compared to a higher dose rate during a shorter time to reach the same absorbed total dose.
- A suggested mechanism behind the radiation induced corrosion of copper is attributed to interactions between hydroxyl radicals and the copper oxide on the copper metal surface. The result is a greatly increased relative surface area and enhanced G-values for hydroxyl radicals at the copper oxide surface.
- The process of radiation induced corrosion of copper in aqueous environment, where the total doses absorbed by copper are equivalent to the total doses expected to be absorbed by the outer canister surfaces during the initial hundred years in a deep repository, is not a direct threat to the integrity of a copper canister for spent nuclear fuel storage.

5. Future work

Based on the results from this study of radiation induced corrosion of copper in anoxic pure water and humid air and argon, some further studies are suggested.

One type of copper was used in this study. It would be interesting to do similar experiments using different purities of copper.

Copper metal become oxidized immediately when in contact with oxygen and therefore further experiments of radiation exposures of pre-oxidized copper samples in humid air and argon will provide data more applicable to reality. Also irradiations of copper in solutions containing chloride, sulfur and carbonates would provide data more related to a deep geologic repository for spent nuclear fuel where copper will be in contact with groundwater.

6. List of abbreviations

Ads. – Adsorbed

AFM – Atomic force microscopy

Arb. – Arbitrary unit

A_S – Solid surface area

BE – Binding energy

B.E.T. – Brunauer-Emmert-Teller

BWR – Boiling water reactor

D – Absorbed total dose (Gy)

E° - Standard reduction potential (V)

G(x) (or G-value) – Radiation chemical yield of product x ($mol \cdot J^{-1}$)

Gy – Gray ($J \cdot kg^{-1}$)

ICP-OES – Inductively coupled plasma-optical emission spectroscopy

IRAS – Infrared reflection absorption spectrometry

k_1 – First-order reaction rate constant

k_2 – Second-order reaction rate constant

PWR – Pressurized water reactor

RH – Relative humidity

SCE – Saturated calomel electrode

SEM – Scanning electron microscopy

UV-Vis – Ultraviolet – visible

XPS – X-ray photoelectron spectroscopy

7. Acknowledgements

The Swedish Nuclear Fuel and Waste Management Co., SKB AB is gratefully acknowledged for financial support.

To both my supervisors, Prof. Mats Jonsson and Prof. Christofer Leygraf, who have been very encouraging, supportive and enthusiastic throughout this project.

To all my colleagues at Nuclear Chemistry: Karin, Claudio, Veronica, Yang, Martin, Sara, Alex, Björn, Helena, Mats, Susanna, Johan, Gabor, Inna, Kristina, Annika and Elin. We've had a lot of fun together!

To my collaborators: Saman, Magnus, Yang, Maddo, Claudia, Billie and Mark. Thank you for the scientific input and the interesting discussions.

To all my friends: you know who you are!

To my family: Thank you for always being there for me.

To Henrik: You are my team mate, computer technician, chef, dry cleaner, concert buddy, cat-daddy, photographer, travel companion and best friend.

8. References

1 www.world-nuclear.org, World Nuclear Association, (accessed 9th of October, 2015).

2 SKB, *Long-term safety for the final repository for spent nuclear fuel at Forsmark. Main report of the SR-Site project.*, Report TR-11-01, Swedish Nuclear Fuel and Waste Management Co., Stockholm, 2011.

3 SKB, *An update of the state-of-the-art report on the corrosion of copper under expected conditions in a deep geologic repository*, Report TR-10-67, Swedish Nuclear Fuel and Waste Management Co., Stockholm, 2010.

4 SKB, *Design, production and initial state of the canister*, Report TR-10-14, Swedish Nuclear Fuel and Waste Management Co., Stockholm, 2010.

5 SKB, *Corrosion calculations report for the safety assessment SR-site*, Report TR-10-66, Swedish Nuclear Fuel and Waste Management Co., Stockholm, 2010.

6 SKB, *Spent nuclear fuel for disposal in the KBS-3 repository*, Report TR-10-13, Swedish Nuclear Fuel and Waste management Co., Stockholm, 2010.

7 F. King, L. Ahonen, C. Taxén, U. Vuorinen and L. Werme, *Copper corrosion under expected conditions in a deep geologic repository*, Report TR-01-23, Swedish Nuclear Fuel and Waste Management Co., Stockholm, 2001.

8 J. Dante and R. Kelly, *Journal of The Electrochemical Society*, 1993, **140**, 1890-1897.

9 S. Lee and R. Staehle, *Corrosion*, 1997, **53**, 33-42.

10 K. P. FitzGerald, J. Nairn, G. Skennerton and A. Atrens, *Corrosion Science*, 2006, **48**, 2480-2509.

11 Y. Feng, K.-S. Siow, W.-K. Teo, K.-L. Tan and A.-K. Hsieh, *Corrosion*, 1997, **53**, 389-398.

12 D. A. Palmer, *Journal of solution chemistry*, 2011, **40**, 1067-1093.

13 F. Samie, J. Tidblad, V. Kucera and C. Leygraf, *Atmospheric Environment*, 2006, **40**, 3631-3639.

14 G. R. Choppin, J. O. Liljenzin and J. Rydberg, *Radiochemistry and nuclear chemistry*, Butterworth-Heinemann, Oxford, U.K., 2nd edn., 1995.

15 J. W. T. Spinks and R. J. Woods, *An introduction to radiation chemistry*, Wiley, 1990.

16 M. Jonsson, in *Recent Trends in Radiation Chemistry* eds. J. F. Wishart and B. S. M. Rao, World Scientific Publishing Co. Pte. Ltd., Singapore, 2010, p. 301.

17 T. Schatz, A. R. Cook and D. Meisel, *The Journal of Physical Chemistry B*, 1998, **102**, 7225-7230.

18 N. M. Dimitrijevic, A. Henglein and D. Meisel, *The Journal of Physical Chemistry B*, 1999, **103**, 7073-7076.

19 N. G. Petrik, A. B. Alexandrov and A. I. Vall, *The Journal of Physical Chemistry B*, 2001, **105**, 5935-5944.

20 E. Chelnokov, V. Cuba, D. Simeone, J. M. Guigner, U. Schmidhammer, M. Mostafavi and S. Le Caër, *The Journal of Physical Chemistry C*, 2014, **118**, 7865-7873.

21 J. A. LaVerne and L. Tandon, *The Journal of Physical Chemistry B*, 2003, **107**, 13623-13628.

22 E. Ekeroth, O. Roth and M. Jonsson, *Journal of Nuclear Materials*, 2006, **355**, 38-46.

23 R. R. Conry, in *Encyclopedia of Inorganic Chemistry*, ed. R. B. King, Wiley, New York, Second edn., 2005, pp. 940-958.

24 W. H. Koppenol and J. F. Liebman, *Journal of Physical Chemistry*, 1984, **88**, 99-101.

25 F. A. Cotton and G. Wilkinson, *Advanced inorganic chemistry*, Wiley Interscience, New York, 3rd edn., 1972.

26 O. Roth and M. Jonsson, *cent.eur.j.chem.*, 2008, **6**, 1-14.

27 C. M. Lousada and M. Jonsson, *Journal of Physical Chemistry C*, 2010, **114**, 11202-11208.

28 C. M. Lousada, A. J. Johansson, T. Brinck and M. Jonsson, *The Journal of Physical Chemistry C*, 2012, **116**, 9533-9543.

29 C. M. Lousada, M. Trummer and M. Jonsson, *Journal of Nuclear Materials*, 2013, **434**, 434-439.

30 A. Hiroki and J. A. LaVerne, *Journal of Physical Chemistry B*, 2005, **109**, 3364-3370.

31 V. M. Goldschmidt, *Naturwissenschaften*, 1932, **20**, 947-948.

32 A. Monod, A. Chebbi, R. Durand-Jolibois and P. Carlier, *Atmospheric Environment*, 2000, **34**, 5283-5294.

33 H. A. Headlam and M. J. Davies, *Free Radical Biology and Medicine*, 2002, **32**, 1171-1184.

34 M. Yang and M. Jonsson, *The Journal of Physical Chemistry C*, 2014, **118**, 7971-7979.

35 K. D. Asmus, H. Moeckel and A. Henglein, *The Journal of Physical Chemistry*, 1973, **77**, 1218-1221.

36 D. W. Johnson and G. A. Salmon, *Journal of the Chemical Society, Faraday Transactions 1: Physical Chemistry in Condensed Phases*, 1975, **71**, 583-591.

37 D. Meyerstein and H. A. Schwarz, *Journal of the Chemical Society, Faraday Transactions 1: Physical Chemistry in Condensed Phases*, 1988, **84**, 2933-2949.

38 Q. Li, P. Sritharathikhun and S. Motomizu, *Analytical Sciences*, 2007, **23**, 413-417.

39 K. Kishore, P. N. Moorthy and K. N. Rao, *International Journal of Radiation Applications and Instrumentation. Part C. Radiation Physics and Chemistry*, 1987, **29**, 309-313.

40 M. Masarwa, H. Cohen, D. Meyerstein, D. L. Hickman, A. Bakac and J. H. Espenson, *Journal of the American Chemical Society*, 1988, **110**, 4293-4297.

41 I. Rusonik, H. Polat, H. Cohen and D. Meyerstein, *European Journal of Inorganic Chemistry*, 2003, **2003**, 4227-4233.

42 J. P. Simpson, *Experiments on container materials for Swiss high-level waste disposal projects. Part II*, Report Nagra Technical Report 84-01, National Cooperative for the Disposal of Radioactive Waste, Wettingen, 1984.

43 C. Corbel, in *Prediction of Long Term Corrosion Behaviour in Nuclear Waste Systems*, eds. D. D. Macdonald and D. Féron, Maney Publishing, London 2003, p. 484.

44 C. D. Litke and F. King, *The corrosion of copper in synthetic groundwater at 150 C. Part 1. The results of short term electrochemical tests*, Report Technical record TR-428, Atomic Energy of Canada Limited, Ontario, 1987.

45 D. T. Reed, V. Swayambunathan, B. S. Tani and R. A. Van Konynenburg, *Materials Research Society Symposium Proceedings*, 1990, **176**, Medium: ED; Size: Pages: (16 p).

46 D. T. Reed and R. A. Van Konynenburg, *Materials Research Society Symposium Proceedings*, 1991, **212**, Medium: ED; Size: 11 p.

47 W. H. Yunker and R. S. Glass, in *Scientific basis for nuclear waste management X: symposium held in Boston, Massachusetts, USA, 1-4 December 1986.*, eds. J. K. Bates and W. B. Seefeldt, PA: Materials Research Society, Pittsburgh, 1986, pp. 579-590.

48 N. G. Petrik, M. N. Petrov and V. G. Fomin, *High Energy Chem.*, 1997, **31**, 308-311.

49 B. M. Carver, D. V. Hanley and K. R. Chaplin, *Maksima-Chemist - a Program For Mass Action Kinetics Simulation by Automatic Chemical Equation Manipulation and Integration Using Stiff Techniques*, Chalk River Nuclear Laboratories, Ontario, 1979.

50 E. A. B. Ross, B. H. J. Bielski, G. V. Buxton, D. E. Cabelli, C. L. Greenstock, W. P. Helman, R. E. Huie, J. Grodkowski and P. Neta, *Journal*, 1992.

51 H. Fricke and E. J. Hart, in *Radiation Dosimetry*, eds. F. H. Attix and W. C. Roesch, Academic Press, New York, 2nd edn., 1966, vol. II, ch. 12, pp. 167-239.

52 *ASTM B825 - 13, Standard Test Method for Coulometric Reduction of Surface Films on Metallic Test Samples*, American Society for Testing and Materials, West Consohocken, PA, USA, 2013.

53 D. L. Perry, *Handbook of Inorganic Compounds, Second Edition*, Taylor & Francis, 2011.

54 Å. Björkbacka, S. Hosseinpour, M. Johnson, C. Leygraf and M. Jonsson, *Radiation Physics and Chemistry*, 2013, **92**, 80-86.

55 B. Lefez, R. Souchet, K. Kartouni and M. Lenglet, *Thin Solid Films*, 1995, **268**, 45-48.

56 G. W. Poling, *Journal of The Electrochemical Society*, 1969, **116**, 958-963.

57 C. D. Wagner, A. V. Naumkin, A. Kraut-Vass, J. W. Allison, C. J. Powell and J. R. J. Rumble, *NIST Standard Reference Database 20, Version 3.4 (web version)*, 2003.

58 Å. Björkbacka, S. Hosseinpour, C. Leygraf and M. Jonsson, *Electrochemical and Solid-State Letters*, 2012, **15**, C5-C7.

59 J. A. Duffy, *Bonding, energy levels, and bands in inorganic solids*, Longman Scientific & Technical, New york, 1990.

60 C. B. Breslin and D. D. Macdonald, *Electrochimica Acta*, 1998, **44**, 643-651.

61 Y.-Y. Su, S. Nakayama and T. Osakai, *corrrev*, 2011, **29**, 51.

62 Å. Bjorkbacka, M. Yang, C. Gasparrini, C. Leygraf and M. Jonsson, *Dalton Transactions*, 2015, **44**, 16045-16051.

63 R. Musat, S. Moreau, F. Poidevin, M. H. Mathon, S. Pommeret and J. P. Renault, *Physical Chemistry Chemical Physics*, 2010, **12**, 12868-12874.

64 S. Le Caër, J. P. Renault and J. C. Mialocq, *Chemical Physics Letters*, 2007, **450**, 91-95.

65 S. Moreau, M. Fenart and J. P. Renault, *Corrosion Science*, 2014, **83**, 255-260.

66 S. C. Reiff and J. A. LaVerne, *The Journal of Physical Chemistry C*, 2015, **119**, 8821-8828.

67 F. A. Miller and C. H. Wilkins, *Analytical Chemistry*, 1952, **24**, 1253-1294.

68 E. A. Secco and G. G. Worth, *Canadian Journal of Chemistry*, 1987, **65**, 2504-2508.

69 R. A. Nyquist and R. O. Kagel, *Infrared Spectra of Inorganic Compounds (3800-45cm−1)*, Academic Press, 1971.

70 H. W. Richardson, *Handbook of Copper Compounds and Applications*, Taylor & Francis, 1997.

71 R. Astumian and Z. Schelly, *Journal of the American Chemical Society*, 1984, **106**, 304-308.

72 P. Wardman and L. P. Candeias, *Radiation Research*, 1996, **145**, 523-531.

73 R. A. Sheldon and J. K. Kochi, in *Metal-catalyzed Oxidations of Organic Compounds*, ed. R. A. S. K. Kochi, Academic Press, 1981, pp. 33-70.

74 I. C. M. S. Santos, F. A. A. Paz, M. M. Q. Simões, M. G. P. M. S. Neves, J. A. S. Cavaleiro, J. Klinowski and A. M. V. Cavaleiro, *Applied Catalysis A: General*, 2008, **351**, 166-173.

75 D. A. Palmer, P. Benezeth and J. M. Simonson, in *Water, steam and aqueous solutions for electric power: Advances in science and technology. Proc. 14th Int. Conf. on the Properties of Water and Steam, 29 August–3 September 2003*, eds. M. Nakahara, N. Matubayasi, M. Ueno, K. Yasuoka and K. Watanabe, Kyoto, Japan, 2004 (2005), pp. 491–496.